Climate Change Detection over Different Land Surface Vegetation Classes

by

Hongyan Dang

M.Sc., Peking University, 1997

A Thesis Submitted in Partial Fulfillment of the
Requirements for the Degree of

Master of Science

in the School of Earth and Ocean Sciences

Supervisor: Dr. Andrew J. Weaver

Abstract

Biosystem variations may occur as a consequence of climate change. Analysis of both modern and paleo-proxy climate data indicates several places on Earth that show biosytem variations possibly resulting from changes in climate. In this thesis, a global land cover classification data set is used to partition the globe into seven regions to study surface temperature changes over different vegetation/surface classes. Statistically significant warming is found from the year 1900 over all regions (except for the ice sheets over Greenland and Antarctica). Outputs from three coupled climate models (CGCM2, HadCM2 and Parallel Climate Model) are then adopted to examine the detection and attribution of surface temperature trends over the various vegetation classes for the past half century. An anthropogenic warming trend is detected in six of the seven regions, which means that anthropogenic activities may have caused detectable influences in the regional surface temperature changes of the past half century. Observed trends are consistent with those simulated in response to greenhouse gas and sulphate aerosol forcing except over tropical forest and water where the models overestimate the warming. The similarity between the resultant scaling factors for each region from the different models underscores the reliability of our detection results.

Table of Contents

List of Tables

List of Figures

Acknowledgements

I wish to thank Prof. Andrew Weaver and Prof. Francis Zwiers for giving me the opportunity to learn a new area of science in this different culture. I appreciate the guidance and mentorship of my supervisor Prof. Andrew Weaver. During the past two years, I learned statistical analysis – a widely used scientific tool that I never used before. It has become quite interesting to me and I will keep learning it in the future. I also had the chance to further develop my background in atmospheric dynamics, such that I cannot imagine challenges as difficult as those I met in the course works at UVic. In these courses, for the first time I became interested in the idealized or conceptual models used in oceanic science and atmospheric science. I was also very impressed by the tough and time-consuming assignments in Dynamic Meteorology and Atmosphere-Ocean System. The most valuable thing that I have learned in the past two years was how to start and expand the research in a scientific topic, how to work effectively, logically, and carefully transfer the results into an accomplishment.

I am grateful to my committee members Dr. Francis Zwiers, Dr. Adam Monahan and Dr. Min Tsao for their commentary on my thesis. I am also grateful to Dr. Nathan Gillett and Dr. Viatcheslav Kharin for their assistance in my thesis work. I also thank Ed Wiebe, Wanda Lewis, Katrin Meissner, Paul Spence, Jeremy Fyke, and the rest of the climate lab for their wonderful help and advice.

Thank-you all my Chinese friends here in Canada for their sincere friendship. I wish to express my gratitude to my family in China, their support and encouragement will be always in my heart.

This research was supported through National Science and Engineering Research Council, the Canadian Foundation for Climate and Atmospheric Studies and the Canadian Climate Variability Research Network, and the Canada Research Chair Program. Infrastructure support from CFI and the University of Victoria is also gratefully acknowledged.

Chapter 1

Research Background and Study Motivation

1.1 Climate change in the 20th and 21st century

1.1.1 Observed changes in surface air temperatures during the 20th century

In the past few years, intense disasters such as floodings, droughts and heat waves have occurred all over the world. The general public naturally associates these extreme climate and weather events with global warming since global warming has been one of the most attention-grabbing scientific phenomenon. From a scientific point of view, the consequences of global warming are still uncertain.

IPCC Third Assessment Report (TAR) (Folland et al. 2001) reports that globally-averaged instrumental records of surface temperatures show increases estimated to be 0.4 – 0.8°C since the late 19th century to the year 2000 (Figure 1.1 (c)). This warming is very unusual compared with the past 1000 to 2000 years of variation shown by proxy temperature data, which are reconstructed from tree rings and ice cores (Mann et al. 1999, Mann and Jones 2003). This warming trend also does not show any sign of ceasing as we enter the 21th century. Annual land-air and sea surface temperature anomalies (Figure 1.2), which are calculated based on the 1961 – 1990 climatology, indicate that the observed temperature anomalies after 2000 still remain highly positive.

In the background of recent global warming trends, there are substantial spatial and temporal variations in surface air temperatures. At the hemispheric scales, sur-

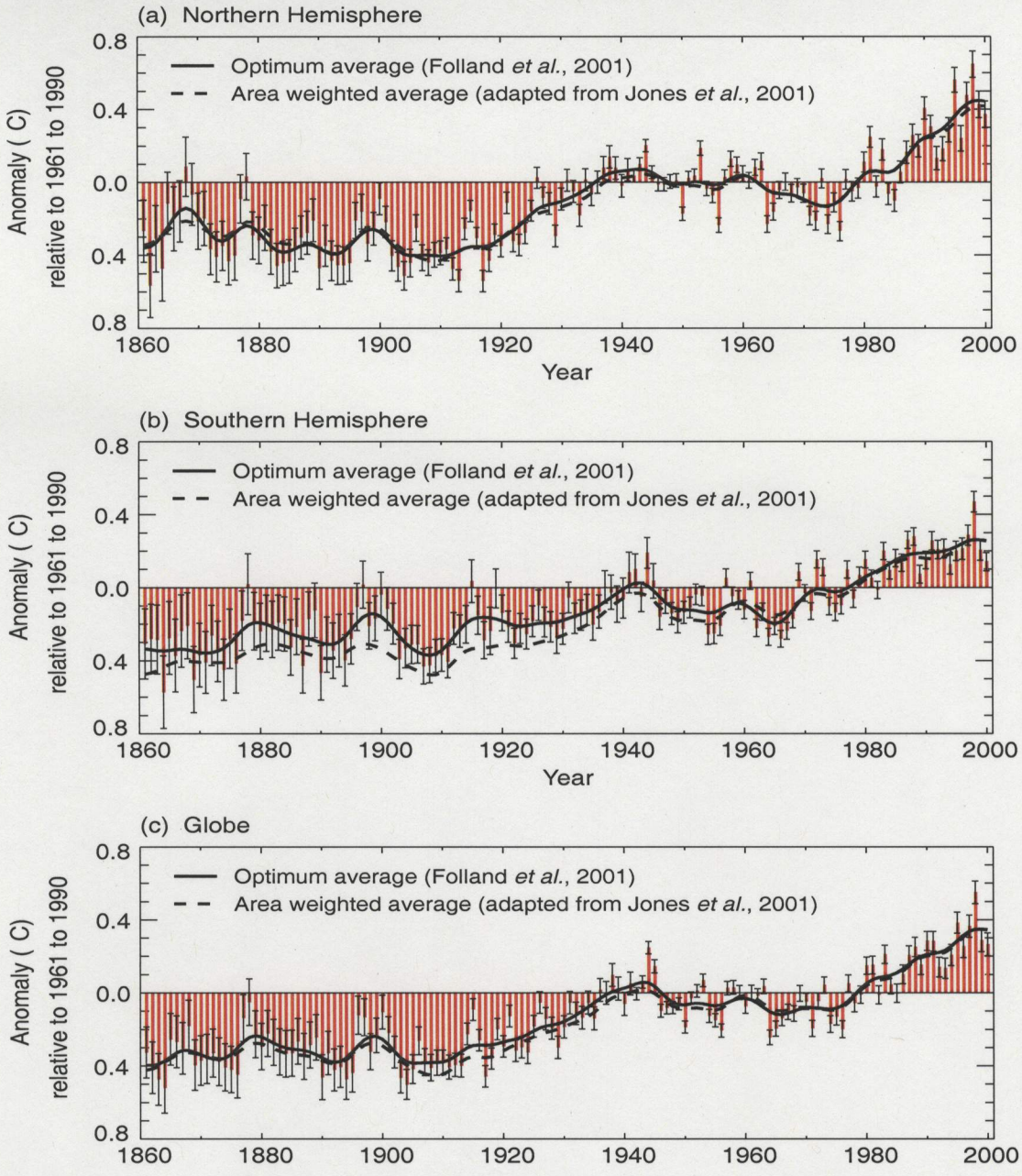

Figure 1.1: **Smoothed annual anomalies of combined land-surface air and sea surface temperatures (°C), 1861 to 2000, relative to 1961 to 1990, for (a) Northern Hemisphere; (b) Southern Hemisphere; and (c) Globe. Reprint of Figure 2.7 from Folland et al. (2001).**

face air temperatures show general warming trends since the start of the Industrial Revolution in both northern and southern hemispheres (Figure 1.1 (a) and (b)). At other planetary-scale levels, such as over land and ocean, average surface air temperatures also show warming trends during the same period (Folland et al. 2001).

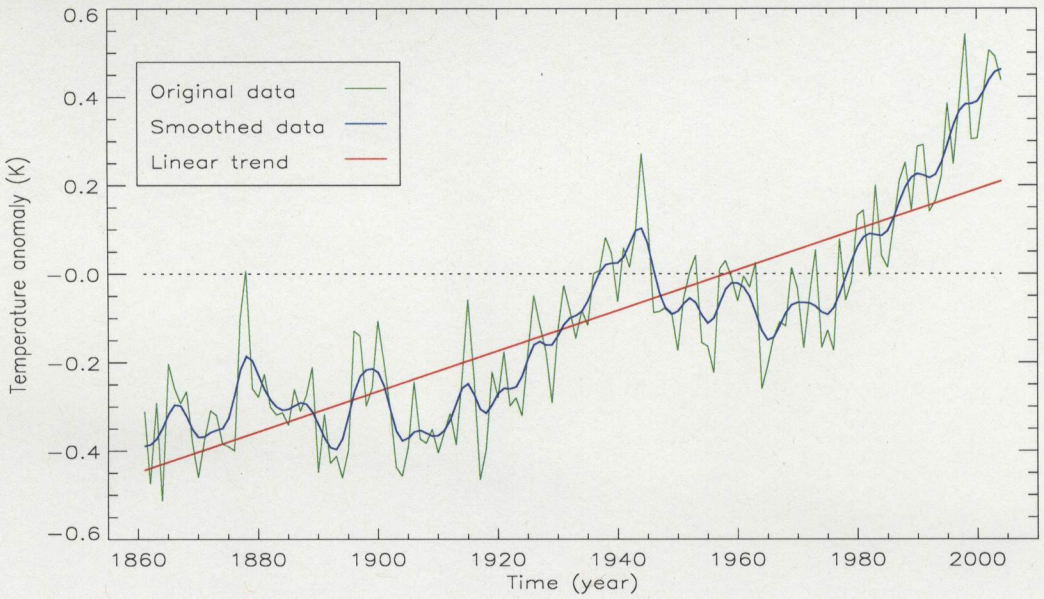

Figure 1.2: **Time series of the globally averaged annual mean temperature anomalies from 1861 to 2004. Smooth curve is a ten-point binomial filter with "padded ends". Original data are available on http://www.metoffice.gov.uk/research/hadleycentre/obsdata/.**

In smaller regions, a surface cooling may exist. Giorgi (2002) examined monthly surface air temperatures from the CRU (Climate Research Unit of the University of East Anglia) dataset and found that the observed temperatures showed significant warming trends throughout the 20th century over the majority of the 22 land regions of sub-continental scale (Figure 1.3). The exceptions were central America, eastern Africa and east Asia in summer. Another surface cooling example is from Doran et al. (2002). Their research suggests a net continental cooling of Antarctica over the period 1966 – 2000 based on spatial analysis of Antarctic meteorological data.

1.1.2 What causes the variations in temperature?

The temperature trends are calculated based on a collection of various local temperature records from the corresponding regions. The temperature record of a place depends on several factors (Peixoto and Oort 1992, Ahrens 1994). The most important factor is latitude, which combines the intensity of incoming solar radiation and

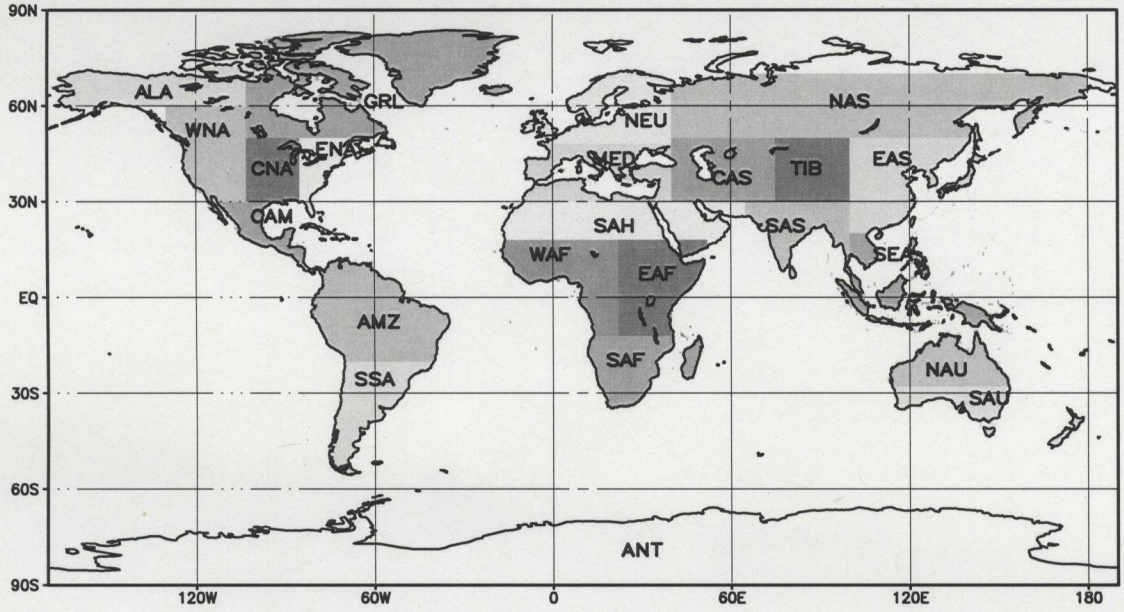

ALA	Alaska	NEU	Northern Europe	NAS	Northern Asia
WNA	Western North America	MED	Mediterranean	TIB	Tibet
CNA	Central North America	CAS	Central Asia	EAS	Eastern Asia
ENA	Eastern North America	SAH	Sahara	SAS	Southern Asia
GRL	Greenland	WAF	West Africa	SEA	South East Asia
CAM	Central America	EAF	East Africa	NAU	Northern Australia
AMZ	Amazonia	SAF	Southern Africa	SAU	Southern Australia
SSA	Southern South America	ANT	Antarctic		

Figure 1.3: **Sub-continental regions used in analysis of surface temperature. Reprinted of Figure 10.1 from Giorgi et al. (2001).**

the length of daylight hours. The other basic factors include the prevailing winds, the underlying surface types such as land or ocean, the influence of ocean currents, the local elevation, the orientation of slopes, local cloud climatology, etc.

These influencing factors determine the variation in surface air temperature distribution and may play an important role in the documented coolings at small spatial scales that are noted above. However the atmosphere as a whole and its average temperature at the Earth's surface are determined by only two factors, i.e. the intensity of the incident sunlight and the greenhouse effect of the atmosphere (Philander 1998). The atmosphere lets in the incident short-wave solar radiation. In the greenhouse effect, the outgoing infra-red radiation from Earth can be trapped by the greenhouse gases in the atmosphere. This process eventually warms the surface atmosphere (Ahrens 1994). In Appendix A, I solved an idealized radiative balance model (Philander 1998) to show the greenhouse gas effect. In this idealized system,

the surface temperature of Earth increases by about 48°C when the greenhouse effect is considered (Appendix A.1 and A.2).

Total solar irradiance has an annual mean variation of approximately 0.08% and is influenced by the solar cycle and other factors such as variations in the Earth's orbit (Ramaswamy et al. 2001). In a period as long as a century or more, but shorter than an ice age, temperature variation due to solar radiation change may still be small. Several studies have shown that the effect of variation in solar radiation (combined with volcanic influences) is small on the warming of the 20th century Earth (Folland et al. 2001). Therefore, it is reasonable to attribute a large amount of the overall warming of surface air temperatures during the 20th century to the increase in the concentration of greenhouse gases in the atmosphere. As for the relation between greenhouse gases and surface temperatures, analysis of paleo-climate data constructed from ice cores shows that during the past 400,000 years, temperature changes are highly consistent with the concentration change of carbon dioxide (CO_2) and methane (CH_4) – the most important greenhouse gases (Figure 1.4) (Petit et al. 1999).

Direct observation and ice-core air measurement shows that the concentrations of major atmospheric greenhouse gases such as CO_2 and CH_4 have increased dramatically during the industrial era (Moore et al. 2001). The abundance of CO_2 has increased from a relatively constant value of 280 ppm (parts per million by volume) in the 1700's up to 370 ppm in the year 2000. The current methane concentration is even further from its value before the Industrial Revolution.

Increased levels of greenhouse gases have been demonstrated by General Circulation Models to be the major contributors to the recent global warming. Early warming in the 20th century may have been influenced by solar variability and a lack of volcanic activity (Hegerl et al. 1997, Tett et al. 1999). However Stott et al. (2000) and Tett et al. (2000) demonstrated, through a coupled atmosphere-ocean model HadCM3, that solar and volcanic only forcing cannot simulate the whole warming trend (Figure 1.5 (a)). Only when well-mixed anthropogenically emitted greenhouse gases (often represented by an equivalent increase in CO_2) are included, is the ob-

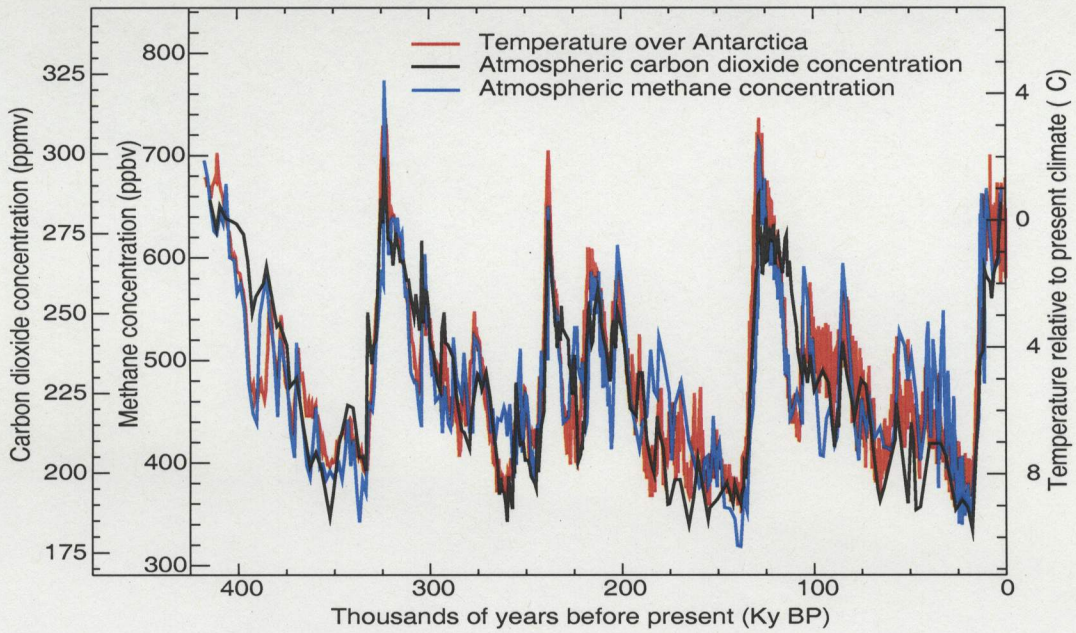

Figure 1.4: **Variations in temperatures, CH_4 and CO_2 concentrations derived from air trapped within ice cores from Antarctica. Reprinted of Figure 2.22 from Folland et al. (2001).**

served warming in the 20th century explained (Figure 1.5 (b)), especially the warming since 1976.

1.1.3 Projected changes in temperatures for the 21st century

Studies conducted with terrestrial/oceanic carbon cycle models or coupled GCM–carbon models suggest that the change of climate and changes in CO_2 levels have had substantial effects on ecosystems (Prentice et al. 2001). For example, one model simulated that C_4 grassland will partially replace the Amazon rainforest (Prentice et al. 2001). It is of interest to estimate the possible future changes in climate and hence determine the potential ecosystem evolution in response to this climate change. Among all natural and anthropogenic climate-sensitive forcings such as solar forcing, volcanic aerosol forcing, changes in greenhouse gas, sulphate aerosol, land-use, mineral dust, black carbon, perhaps the most important one is the change in greenhouse gas concentrations.

The simple idealized model used in Appendix A can still be used to estimate the

changes in surface temperatures forced by increased greenhouse gases. In this model, a doubling of greenhouse gas concentrations in the atmosphere has a risk of causing the Earth's surface temperature to increase about 32°C. Several shortcomings of this model make the estimated temperature extremely high (Appendix A.4).

Future climate changes until 2100 can be more realisticly assessed by complicated climate models such as the Atmosphere-Ocean General Circulation Model that includes a range of more realistic scenarios (external forcing estimations) for projected changes, mainly in greenhouse gas concentrations and sulphate aerosol loadings (Cubasch et al. 2001). Although uncertainties exist and different models may produce different results under various scenarios (Weaver and Zwiers 2000, Zwiers 2002), there is still great similarity between the projections of a global warming for the near term. The climate of such a period "results from the climate's adjustment to changes in the greenhouse-gas content of the atmosphere that have already occured, due to the large thermal inertia of the oceans" and indicates that the influences of greenhouse gases and sulphur dioxide partially offset each other (Zwiers 2002). In the long run, the uncertainty range of the warming trend is large. In 2100, relative to 1990, projected surface air temperature increases could range from 1.0 to 5.8°C (combined from two ranges given in Cubasch et al. (2001), i.e. $1.0 \sim 3.5$°C and $1.4 \sim 5.8$°C).

The IPCC TAR concluded that "most of the warming observed over the last 50 years is attributable to human activities" (Mitchell et al. 2001). As mentioned at the start of this section, if the substantial observed changes in ecosystems under observed historical climate change can be linked to human activities, further changes in ecosystems can be expected under continued anthropogenic global warming in the future. What's more, we may still expect anthropogenic impacts on the future ecosystems regardless of whether these impacts have already been documented.

1.1.4 Detection and attribution of climate change

The anthropogenic influence on the Earth's surface air temperature changes has been intuitively analyzed in Section 1.1.2, and it can be further quantitatively studied through a climate change detection and attribution study.

The observed temperature changes can result from temperature variation arising from climate variability caused by the natural interactions between the five major components of the climate system. They can also be the consequence of climate changes which are driven by external mechanisms that influence one or more of the climate system components (Hasselmann 1997). As previously mentioned in Section 1.1.3, the external forcings have both natural and anthropogenic sources. Natural forcings include fluctuations of the solar constant and aerosol emissions to the atmosphere from volcanic activities. Anthropogenic forcing indicates human-activity-driven concentration changes in atmospheric components such as greenhouse gases and sulphate aerosols as well as changes in underlying surface conditions of the atmosphere due to land-use and deforestation.

The observed space-time-dependent climate variations since the late 19th century are not believed to be generated by the ensemble of climate variability or natural external forcing alone (Section 1.1.2). A signal detection and attribution study can statistically distinguish, from the natural variability, the significance of the detection of climate change signal patterns and the consistency level of climate change attribution to external forcing mechanisms (Hasselmann 1993, 1997). Here, the exact meaning of detection is "the process of demonstrating that an observed change is significantly different than that which can be explained by natural internal variability"; attribution is the process of attributing a detected climate change signal to the involved external forcings (Mitchell et al. 2001).

In the IPCC TAR, climate change detection and attribution studies have mainly concentrated on the global scale, with the issue of regional-scale detection still in its infancy (Mitchell et al. 2001). Several global climate change detection and attribution studies have been conducted. Tett et al. (1999), Stott et al. (2001) and Mitchell et al. (2001) found that the anthropogenic emitted greenhouse gases and tropospheric sulphate aerosols have had a detectable effect on surface air temperatures in the latter half of the 20th century. The research of Barnett et al. (2001) and Levitus et al. (2001) suggests a consistency between the observed ocean heat-content changes of the past half century and those that are simulated by coupled climate models in response

to anthropogenic forcing. Gillett et al. (2003) found that anthropogenic greenhouse gases and sulphate aerosols have had a detectable influence on sea-level pressure over the second half the 20th century. Similar climate change detection and attribution studies can also be found in Hegerl et al. (1997), Hegerl et al. (2003) and Hegerl et al. (2004).

Regional-scale detection remains difficult because signal to noise ratios diminish with scale (Stott and Tett 1998). Recently, however, a number of studies concerning the potential impact of climate change on smaller scales have appeared. Through the analysis of indices of several continental patterns, Karoly et al. (2003) found that the observed 1950-1999 North American surface temperature trend is consistent with the modelled response associated with anthropogenic changes in greenhouse gases and sulphate aerosols. In addition, the combined influence of anthropogenic greenhouse gas and sulfate aerosol forcing on surface temperature changes was found to be detectable on the continental scale for the second half of 20th century (Zwiers and Zhang 2003). Stott (2003) also found that an increasing surface temperature trend due to greenhouse gases could be detected in six continental regions. Zhang et al. (2005) found clear detectable anthropogenic forcing effects in nine spatial regions from global scale to country-wide (such as southern Canada and China). Finally, Gillett et al. (2004a) demonstrated that anthropogenic greenhouse gases and sulphate aerosols have had a detectable influence on fire-season warming of the Canadian forest region, while Karoly and Wu (2005) detected anthropogenic warming trends over many parts of the globe at scales of 500 km.

1.2 Research motivation

The purpose of this research is to quantitatively understand the anthropogenic influence on recent surface temperature changes at regional scales through a detection and attribution study. The regions used here are divided based on the biome features of the surface types of the region.

It is well known that different land surface types can affect climate in a variety of

ways, perhaps the most important being their effects on surface albedo, evapotranspiration, and the terrestrial carbon cycle. In addition, the regional biomass distribution is known to respond to, as well as feed back upon, climate change. Paleo-proxy records and paleoclimate modelling studies have been particularly helpful in assessing such vegetation responses and feedbacks (McAvaney et al. 2001, Meissner et al. 2003). Over long periods, climate change can cause important changes in the geographic distribution and abundance of major land cover types and animal habitats (Melillo 1999, Parmesan and Yohe 2003, Thomas et al. 2004). Hughen et al. (2004), for example, found a rapid shift between arid grassland and wet forest in the Cariaco region during deglacial high-latitude North Atlantic climate oscillations. Meta-analysis conducted by Root et al. (2003) has also revealed a discernible trend in the population of both animals and plants as a consequence of climate warming over the past century. O'Reilly et al. (2003) provided further evidence that climate warming has the potential to modify aquatic biota and ecosystems through its influence on the stability of the water column and hence nutrient transport.

Temperature changes over different biotic regions play an important role in climate impacts and feedbacks within the climate system. For example, the atmospheric methane concentration has a close relationship to the atmospheric temperature record (Wuebbles and Hayhoe 2001), and the emission of methane from melting tundra increases in association with surface warming of this region. Different biota also respond to surface temperature changes through different mechanisms. As such, the analysis of simulated and observed changes over these separate regions may enhance our understanding of biotic feedbacks operating within the climate system. Since temperature changes over specific biome regions have not been systematically studied, it is necessary to systematically study how the observed surface temperatures change over major biome regions. It is also necessary to determine if the observed change (signal) in the past century is significantly different from that which can be explained by natural climate variability and to study if the anthropogenic activities have caused detectable effects in these regional temperature changes.

1.3 Outline of the research

In Chapter 1, we learned that there is an unusual global surface temperature warming from the start of the Industrial Revolution. There is a very high probability that this unusual warming largely results from the increase in the abundance in anthropogenic emitted greenhouse gases to the atmosphere. However, changes in surface air temperatures on regional scales show both warming and cooling trends. We also learned that there is substantial evidence to show that the Earth's ecosystem responds to changes in its surrounding climate, especially changes in temperature. Temperature changes over specific biome regions have not been systematically studied. Therefore, in Chapter 2, temperature conditions over specific biome regions will first be systematically examined and assessed for significant warming or cooling trends over the major biotic regions on Earth.

To understand whether these observed temperature changes are a result of natural internal variability of the climate system, or due to external forcings, Chapter 3 is dedicated to an investigation of the influence of anthropogenic emitted greenhouse gases and sulphate aerosols on regional temperature changes. A detection and attribution study is conducted to examine if the anthropogenic emission of the combined greenhouse gases and sulphate aerosols or the greenhouse gases alone have had a detectable influence on the regional temperature changes of the second half of the 20th century. In this section, there is also a comprehensive discussion of the optimal fingerprinting method.

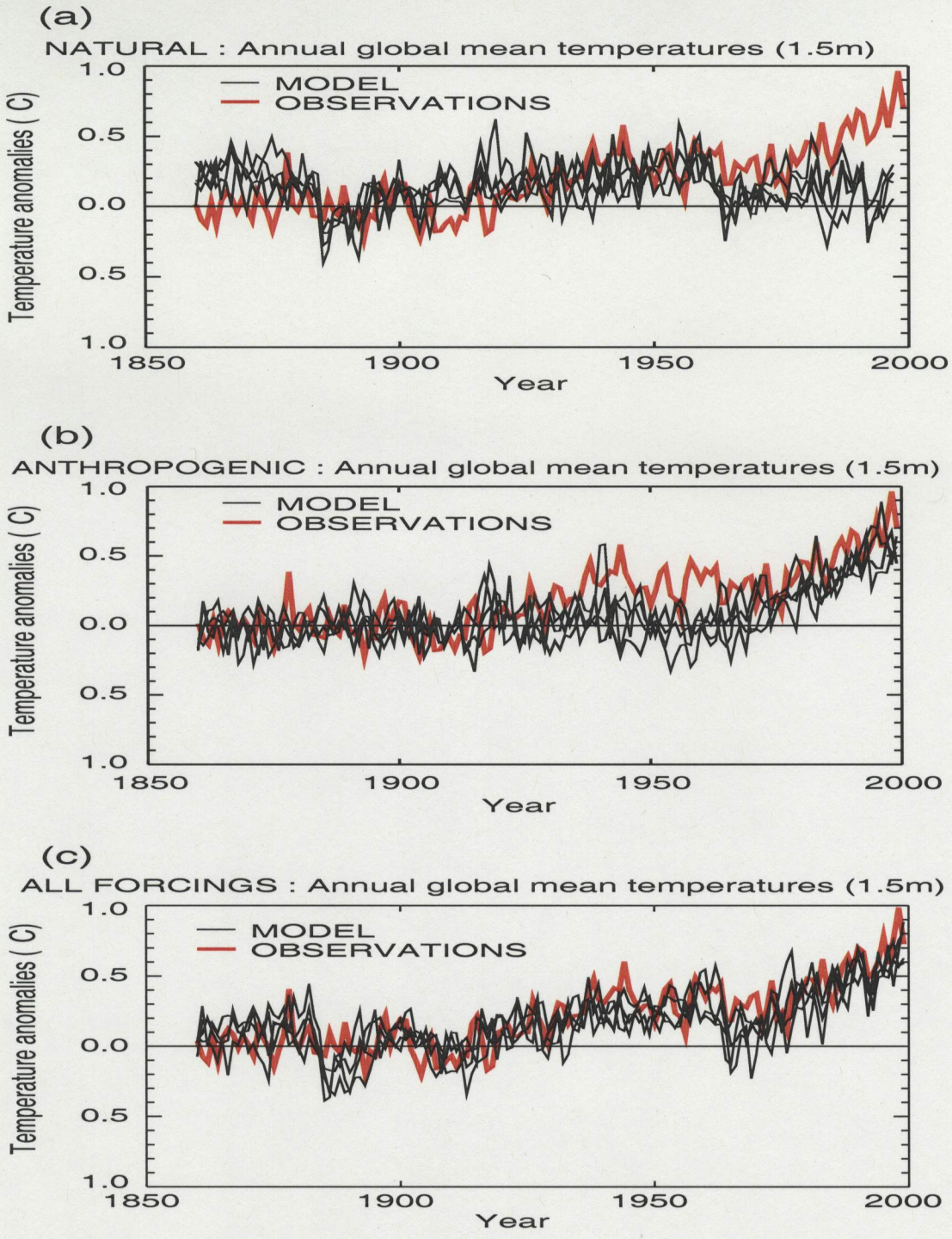

Figure 1.5: Global mean surface temperature anomalies relative to the 1880 to 1920 mean from the instrumental record, compared with ensembles of four simulations with a coupled ocean-atmosphere climate model involing (a) solar and volcanic forcing only, (b) anthropogenic forcing including well mixed greenhouse gases, changes in stratospheric and tropospheric ozone and the direct and indirect effects of sulphate aerosols, and (c) all forcings, both natural and anthropogenic. Reprinted from Figure 12.7 in Mitchell et al. (2001).

Chapter 2

Climate Change over Different Land Surface Vegetation Classes

2.1 Partitioning of land surface types

In this thesis, the National Aeronautics and Space Administration (NASA), International Satellite Land Surface Climatology Project (ISLSCP), and Global Data Sets for Land-Atmosphere Models (GDSLAM) vegetation class data set (DeFries and Townshend 1994) is adopted as the basis to define the biotic regions. The NASA-ISLSCP-GDSLAM-Vegetation class dataset describes the geographic distribution of 16 major land cover types on a $1°\times1°$ (latitude $\times$ longitude) grid, based on data collected in 1987 (upper panel of Figure 2.1). Though the c4 grassland is named as a surface type, its distribution is not included in the dataset, thus, the original dataset only includes 15 kinds of surface types. In addition, sea ice is not identified separately, but rather was included in global water.

Allowing for the analysis of climate change on scales sufficiently large to allow regional scale climate change detection, the original 15 surface types are re-grouped into seven larger different types (Table 2.1): (1) water (including sea ice), (2) tropical forest (including subtropical forest), (3) temperate forest,(4) bare ground (including desert, bare ground, and grassland), (5) tundra, (6) cultivated land, and (7) continental ice (bottom panel of Figure 2.1). As the purpose of this thesis is to analyze regional temperature changes, when defining the subregions, a major consideration is the latitude and spatial continuity of the candidate smaller surface classes. Some other features are also considered, but generally it is not possible to consider all influencing factors. For example, when grouping shrubs, desert, bareground, c3 wooded

Table 2.1: **Partitioning of 16 land surface classes, as identified by NASA-ISLSCP-GDSLAM-Vegetation class dataset, into 7 re-grouped classes**

Original surface class number	Original surface class type	Re-grouped surface class type	Re-grouped number
0	Water	Water	1
1	Broadleaf forest	Tropical forest	2
2	Broadleaf deciduous		
6	Forest and woodland		
7	Wooded c4 grassland		
3	Mixed coniferous &broadleaf deciduous	Temperate forest	3
4	Coniferous forest &woodland		
5	High latitude deciduous		
9	Shrubs and bareground	Bare ground	4
11	Desert and bareground		
14	C3 wooded grassland		
15	C3 grassland		
10	Tundra	Tundra	5
12	Cultivated land	Cultivated land	6
13	Ice	Continental ice	7
8	C4 grassland	—	—

grassland and c3 grassland together, both the spatial continuity and similar albedos are considered, while the surface roughness and evapotranspiration have been ignored.

2.2 Analysis of regional surface air temperature changes

The surface air temperature trends over the seven broad classes defined in Section 2.1 were analyzed using the variance-adjusted 1870 – 2004 monthly mean surface temperature anomaly dataset (HadCRUT2v – Jones et al. (2001)) with a spatial resolution of 5°×5° (latitude × longitude). This monthly dataset provides temperature anomalies relative to 1961 – 1990. The latitudes and longitudes of the grid points for the temperature data coincide with those of surface cover type data on every 5°×5° grid.

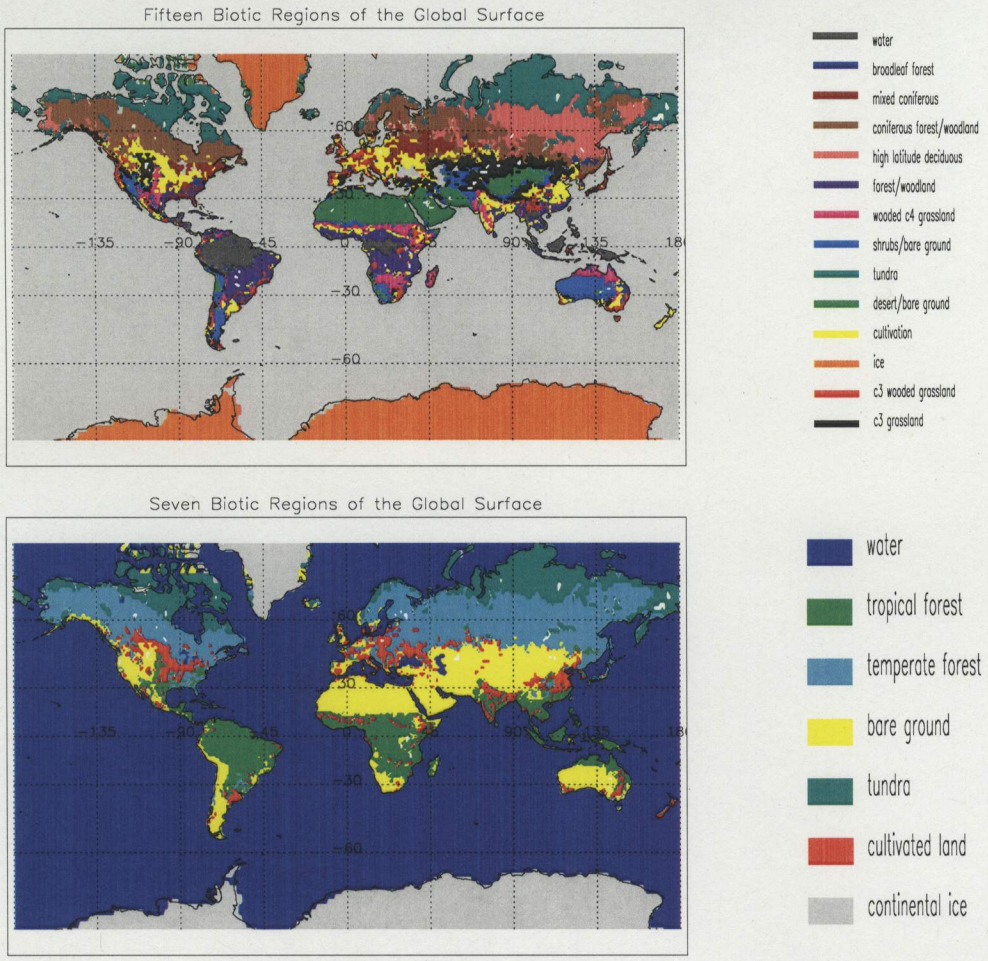

Figure 2.1: **Upper: Distribution of original 15 surface types in the NASA-ISLSCP-GDSLAM-Vegetation class dataset. Bottom: Re-grouped seven subregions based on different vegetation/surface types.**

Since the value of the temperature anomaly on each point represents the average temperature anomaly of the whole 5°×5° area around this point, all 25 of the 1°×1° vegetation grid boxes in this area were assigned the same temperature anomaly as the center point. In this way there was a corresponding temperature anomaly record for each vegetation box. Figure 2.2 shows that the re-allocated 1°×1° temperature distribution (bottom panel) is virtually identical to the 5°×5° temperature distribution (upper panel).

Area-weighted, annual-mean temperature anomalies were calculated for each of the seven biotic regions. The weighting coefficient at the corresponding latitude is given by $cos\theta$, where θ is the latitude (in radians). The temperature anomaly for

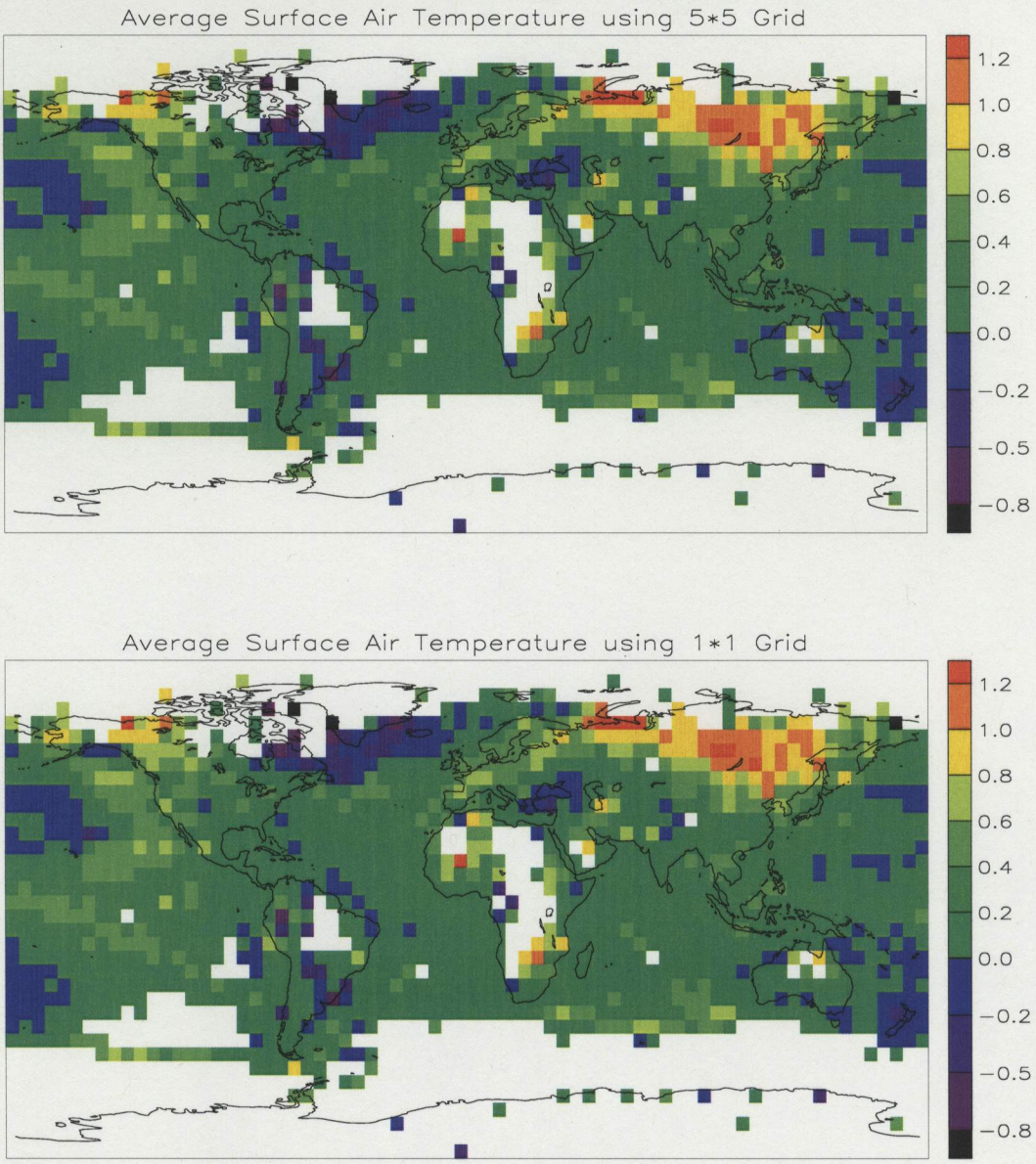

Figure 2.2: **An example of decadal average surface air temperature anomalies using 5°×5° (latitude × longitude) box (upper) and 1°×1° (latitude × longitude) box (lower) for 1986 – 1996 dataset.**

a specific grid box was treated as missing if even one month within the year was missing at this grid. An ordinary least squares fit regression analysis was applied to estimate the linear trends of temperature over these regions from the start of the 20th century and from the mid-20th century. A student's t-test was applied to test the

Table 2.2: **Autocorrelation coefficients of the 7 regional surface air temperature anomalies for the time series lag-1, lag-2, lag-3**

Surface class number	Surface class type	lag-1	lag-2	lag-3
1	Water	0.65	0.38	0.36
2	Tropical forest	0.48	0.17	0.22
3	Temperate forest	0.14	0.14	-0.04
4	Bare ground	0.58	0.44	0.40
5	Tundra	0.18	0.17	0.11
6	Cultivated land	0.31	0.14	0.07
7	Continental ice	0.56	0.42	0.38

null hypothesis that the temperature trends were not changing during the period of examination (von Storch and Zwiers 1999).

The autocorrelation coefficients of the seven regional surface air temperature anomalies indicate that the regional mean temperature time series do not behave as white noise (Table 2.2) (von Storch and Zwiers 1999). The lag-1 year, lag-2 year, and lag-3 year autocorrelations are significantly different than zero indicating that the annual mean temperature anomaly is quite persistent. Thus, when estimating the 95% confidence intervals, an effective sample size $N_e = n(1-\rho)/(1+\rho)$ is assumed, where n is total years of observations and ρ is the lag-1 autocorrelation coefficient of annual anomalies. Assuming the process is auto-regressive (AR-1) is reasonable – the estimated effective sample N_e size is reduced a bit since the lag-1 correlation coefficient is a bit bigger due to external forcings. Tests using a smaller number of effective degrees of freedom will be more conservative (personal communication with Francis Zwiers).

The regression coefficients, which are given in Table 2.3, reflect a general warming trend from 1900 to 2004 over all regions, with warming trends being even greater over the period from 1950 to 2004. No significant warming trend was observed over the continental ice sheet region during either time period. The warming trends in the other six surface classes were found to be statistically significant at the 5% significance

Table 2.3: **Regression coefficients for regional surface temperature trends over two 20th century time periods**

Surface class number	Surface class type	1900 – 2004	P-value	1950 – 2004	P-value
1	Water	0.67±0.16	<0.05	0.77±0.38	<0.05
2	Tropical forest	0.61±0.19	<0.05	1.12±0.43	<0.05
3	Temperate forest	1.07±0.29	<0.05	2.26±0.64	<0.05
4	Bare ground	0.87±0.26	<0.05	1.86±0.50	<0.05
5	Tundra	0.95±0.41	<0.05	1.98±0.84	<0.05
6	Cultivated land	0.72±0.21	<0.05	1.37±0.57	<0.05
7	Continental ice	0.15±0.97	0.75	0.33±0.77	0.39

The amplitude of the surface temperature trends (°C/100yr) for the periods from 1900 to 2004 and from 1950 to 2004; ±95% confidence intervals and the P-values for trend tests in the seven biotic classes.

level. As shown in Table 2.3, the P-values for each of these six regions all meet the threshold 0.05. For these six regions, there is strong evidence in support of the warming trends for both periods of study. The warming trends increased in the second half of the 20th century (Figure 2.3). The greatest warming happened over tundra and the temperate forest region and these trends are more apparent from 1950 onward. This is consistent with Giorgi et al. (2001) whose results suggest that nearly all land areas warm more rapidly than the global average, especially at high latitudes. The high latitude land region warming in the cold season plays an important role in its annual change (Giorgi et al. 2001), but seasonal changes are not a concern in this thesis. Furthermore, the warming in the water region is smaller than over the land areas during this period, as expected from the high heat capacity of water relative to land.

Though the trends over all regions are constant, generally, the uncerainty in the continental region is too large to determine whether the trend is significant at the region. The smaller the fraction of the total number of 1°×1° boxes that is used to calculate trend for that region, the larger the sampling variability in the regional mean temperature is. This can be clearly reflected by the largest uncertainties in the continental ice region. Although the area of the continental ice region is much larger

than some of the other regions, the available instrumental records that can be used to do temperature trend analysis are always less than those of the other regions due to the scarce observation in this region. The fractions of the available data in all regions increase with time as more and more instrumental observations are available.

There is a period of cooling from 1946 to 1975 in all regions except bare ground (Figure 2.4). These regional coolings are generally consistent with the global changes of the same period. The global cooling of this period can be reproduced with climate models only when natural forcing mechanisms are also included in addition to the greenhouse gas and sulphate aerosol concentration changes in climate simulations of the 20th century (Figures 1.5 (c)). Therefore natural factors such as solar or volcanic activities may play an important role in the regional cooling shown in Figure 2.4. In addition, cooling in the continental ice region during the period 1930 – 1975 was found to be statistically significant (-0.31±0.12°C/decade) with the 95% confidence interval. Unfortunately, it is still unclear whether aggregation of station data over the continental ice region into 5°×5° boxes is credible in light of the very sparse data available to compute the spatial average over the whole region.

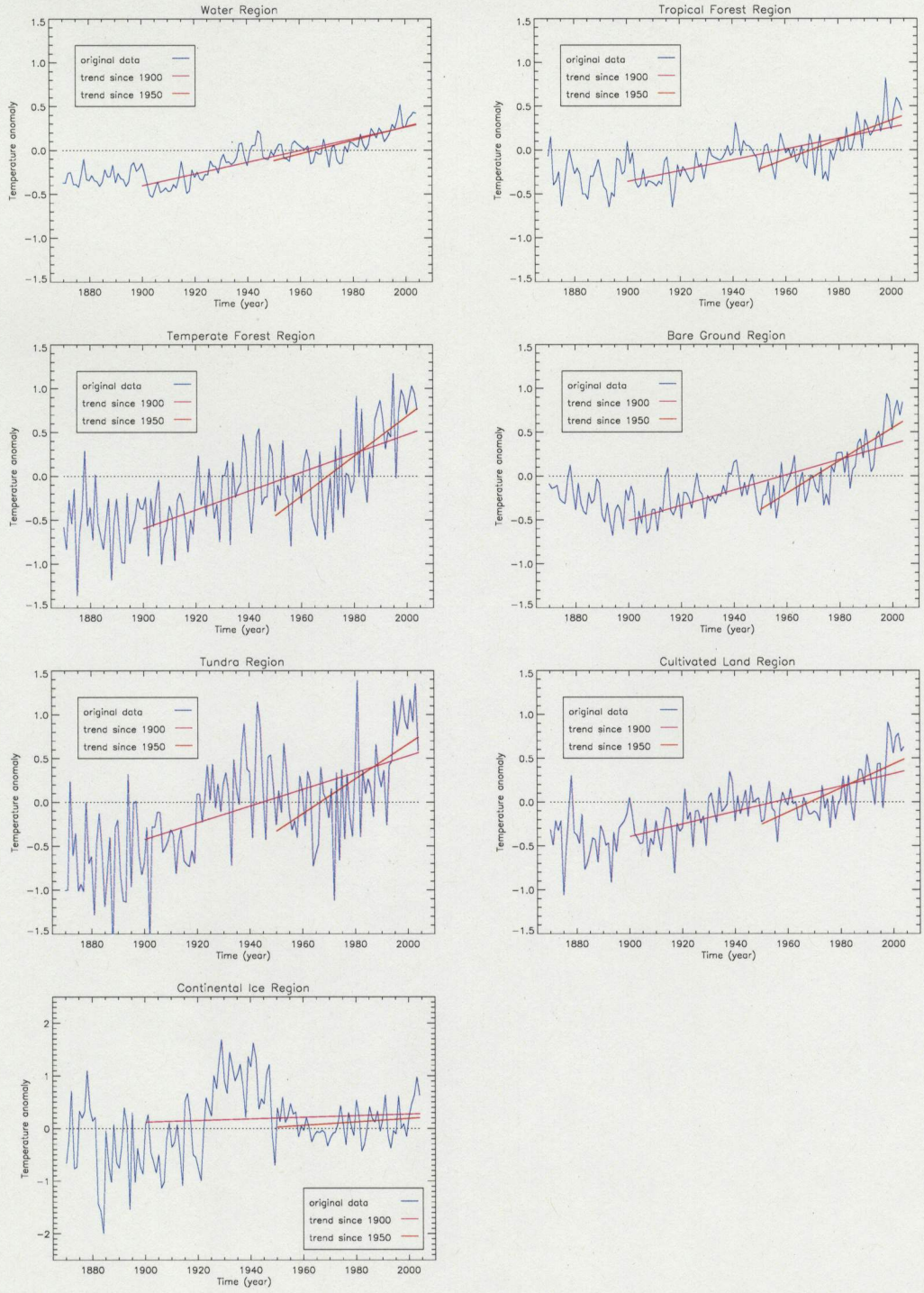

Figure 2.3: **Surface warming trends in 6 of 7 biotic regions, as shown by temperature anomaly data and linear trends lines for two 20th century time periods.**

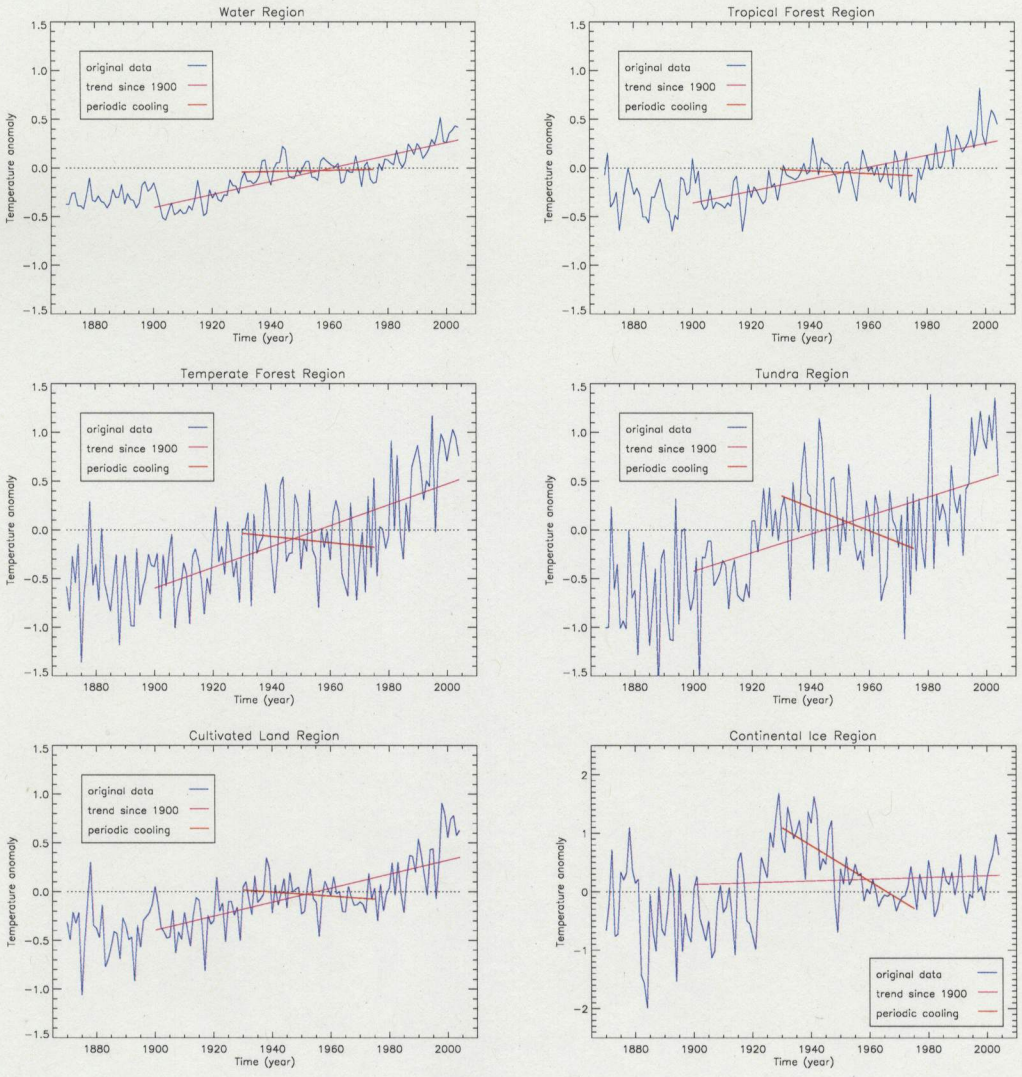

Figure 2.4: **Regional-average surface cooling from 1946 to 1975 in five biotic regions as shown by temperature anomaly data and linear trend lines for 1946 to 1975. Regional-average surface cooling from 1930 to 1975 over the continental ice region.**

Chapter 3

Detection and Attribution Analysis of Regional Climate Change Using Optimal Fingerprinting

3.1 Introduction

In this section, a detection and attribution analysis using optimal fingerprinting is carried out to quantitatively examine the response of the observed temperature changes to anthropogenic greenhouse gases and sulphate aerosols.

According to the definitions of climate change detection and attribution given in Section 1.1.4, we need to separate climate variability and the climate changes from the mean climate state. Therefore, I will first provide a brief introduction regarding the process of this separation, and illustrate how climate variability and climate changes affect the quantitative detection and attribution analysis.

A quantitative detection and attribution analysis requires the exact space-time structure of climate variability and climate changes (Hasselmann 1997). In practice, a spatially and temporally continuous climate trajectory $\mathbf{U}$ can be decomposed into a finite dimensional phase space with dimensions $m \times n \times t$, where m is the total number of latitudes, n is the total number of longitudes, and t indicates the total number of time repetitions. Due to this huge dimension, the space-time covariance structure of natural variability is difficult to be estimated. An EOF representation of $\mathbf{U}$ can be adopted to effectively diminish the dimension and to filter minor variations which only contribute "noise" for a climate change detection and attribution study (Hasselmann

1997, Hegerl et al. 1997).

The task of detection and attribution studies is to determine whether the observed climate change signal is internally generated by the climate system itself or forced by one of the various external factors. For this purpose, we are going to assume internal climate variability and the responses to the various external forcings contribute linearly to observed climate change. It has been shown acceptable at least for greenhouse gas and aerosol forcing to introduce linear assumptions (Santer et al. 1995, Gillett et al. 2004b, Hasselmann 1993, 1997, 1998, Hegerl et al. 1997, Allen and Tett 1999, Allen and Stott 2003) for $\mathbf{U}$ such that

$$\mathbf{U} = \mathbf{U^{var}} + \mathbf{U_1^{chn}} + \mathbf{U_2^{chn}} + ... + \mathbf{U_k^{chn}}, \tag{3.1}$$

where $\mathbf{U^{var}}$ is internal climate variability (also called noise) and $\mathbf{U_i^{chn}}$ is climate change (also called signal) caused by the $\mathbf{i}^{th}$ $(i = 1, 2, ..., k)$ external forcing mechanism. So far, these linear accumulations ignore two kinds of nonlinear interactions: nonlinear interactions between climate variability and climate change, and nonlinear interactions between different climate changes. The k climate change signals are generally additive, while in practice the response to different forcing patterns computed by a given model can be quite similar (Hegerl et al. 1997, North and Stevens 1998, Tett et al. 1999, Mitchell et al. 2001). For example, the simulated spatial pattern of the greenhouse gases forcing might be similar to that of the sulphate aerosol forcing, although the amplitudes of these responses would be different, and the responses could well be of opposite sign (positive in the case of greenhouse gases forcing and negative in the cases of aerosol forcing). For a successful detection, Hasselmann (1997) indicated that k should not be greater than three. When discriminating a climate change signal in the observed data, the significance of the signal decreases as the dimension of the problem increases (Bell 1986). Based on prior knowledge regarding the physical mechanism of the influences, the main anthropogenic influences expected to have the largest influence on the climate system are greenhouse gases and aerosol emissions, deforestation, and land-use changes. Also note that the chosen $\mathbf{U}$ for detection and

attribution studies need not be a "dynamically integrated" climate state, although this might reduce detection power (Hasselmann 1993). Surface temperature, vertical temperature, precipitation, and other variables or indices have been individually used for this study in recent years.

To complete the detection and attribution analysis, the following components are necessary: observations, externally forced climate changes, and climate internal variability. The externally forced climate state and internal variability need to be simulated from climate models (simple models or GCMs). It may not be appropriate to estimate climate variability from observed records because currently available instrumental data might not be long enough (less than 150 years) to cover variability at all time scales, and their spatial coverage is limited. It is also hard to accurately exclude potential externally forced climate changes from the observations. Paleoclimate proxy data restructed from tree rings, coral records, and ice cores are also not suitable for estimating climate variability, the reason is that the proxy data are sparsely scattered on Earth and largely indicator of local climate variations (Barnett et al. 1999).

Figure 3.1 illustrates the relationship between climate variability and climate change signals in a two-dimensional vector space. As indicated, once the end point of $\mathbf{U}^{obs}$ (or $\mathbf{U}^{rtr}$ starting from end point of $\mathbf{U}^{obs}$) lies in the consistency ellipse of $\mathbf{U}^{var}$, the retrieved climate change signal is said to be consistent with (caused by) $\mathbf{U}^{var}$, in that there is no detectable climate change in the observation. If $\mathbf{U}^{prd}$ lies outside of the consistency region of $\mathbf{U}^{var}$, then it implies that a climate change due to the external forcing is detected. If the observation lies in the consistency region of $\mathbf{U}^{prd}$ (not consistent with climate change forced by other sets of external factors) and out of consistency region of $\mathbf{U}^{var}$, the observed climate change is then attributed to this forcing mechanism.

Figure 3.2 shows five outcomes for these three vectors (or more than three, if more externally generated climate state are included) based on the above deterministic judgment of detection and attribution (Hasselmann 1997). Their quantitative relationships can be revealed by projecting $\mathbf{U}^{obs}$ onto $\mathbf{U}^{prd}$ space (Allen and Tett 1999,

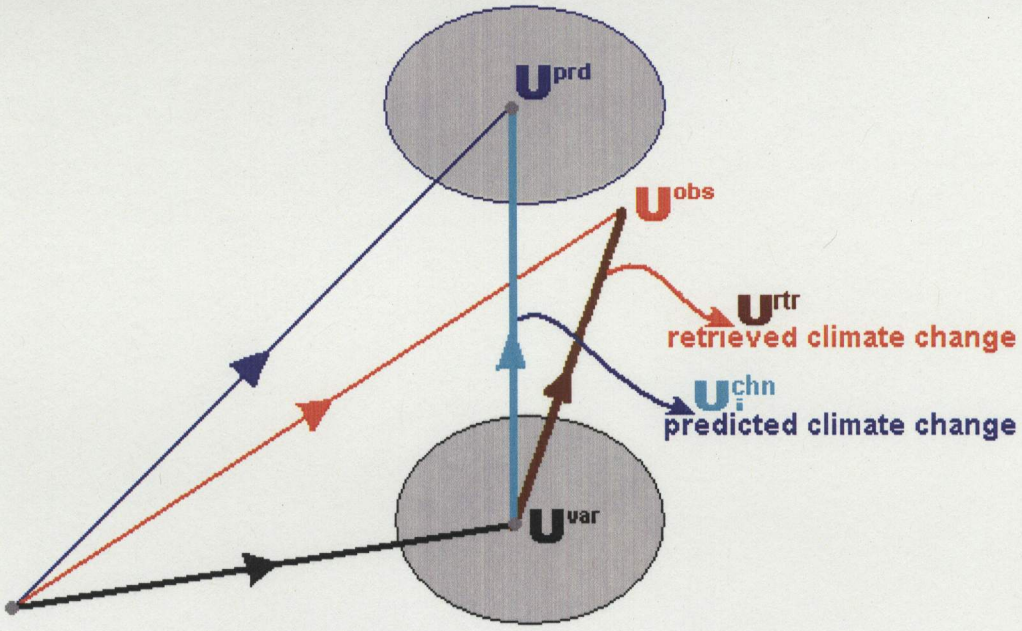

Figure 3.1: **Climate internal variability (noise) U^{var}, observed climate state U^{obs}, and model simulated climate state U^{prd} forced by some external forcing mechanism. Ellipses indicate regions consistent with respective inner vectors. This vector representation is an extension of Hasselmann (1997).**

Mitchell et al. 2001, Stott et al. 2001, Allen and Stott 2003). In Case 1 of Figure 3.2, U^{obs} is not consistent with U^{var}, there is a detected climate change in the observation and $\beta > 0$ (for a definition of β, see Section 3.2); U^{obs} is not consistent with the signal forced by the external mechanism – β is inconsistent with 1. In Case 2 of Figure 3.2, U^{obs} is not consistent with U^{var}, $\beta > 0$; it is consistent with predicted climate change forced by external mechanism-1, but not consistent with all other responses to external mechanisms other than mechanism-1, therefore, an attribution of the observed climate change to mechanism-1 is declared. In Case 3 of Figure 3.2, the detected observed climate change (not consistent with U^{var}, $\beta > 0$) is consistent with more than one external forcing mechanisms, thus, no attribution can be declared. In Case 4 of Figure 3.2, U^{obs} is consistent with both U^{var} and U^{prd}, the confidence region of β includes both 0 and 1, there is neither detection nor attribution evidence. In Case 5 of Figure 3.2, U^{obs} is consistent with U^{var}, but not consistent with any externally forced signals, or predictions and the observation have opposite directions; β's confidence

region includes 0, or upper limit of β is less than 0. Given that model system errors have been ignored then all uncertainties about the structure and magnitude will come from internal variability, i.e. from model control simulation. Therefore, the predicted climate change signal will be assumed to be realistic (Hasselmann 1993, Hegerl et al. 1997). In addition, the influence of measurement errors in detection analysis has been shown to be small (Hegerl et al. 2000). Therefore, each set of analysis shows a distribution of internal variability, (assumed to be Gaussian or other known distributions) (Hegerl et al. 1997, Allen and Stott 2003). The confidence limits for estimated climate change signals can thus be determined.

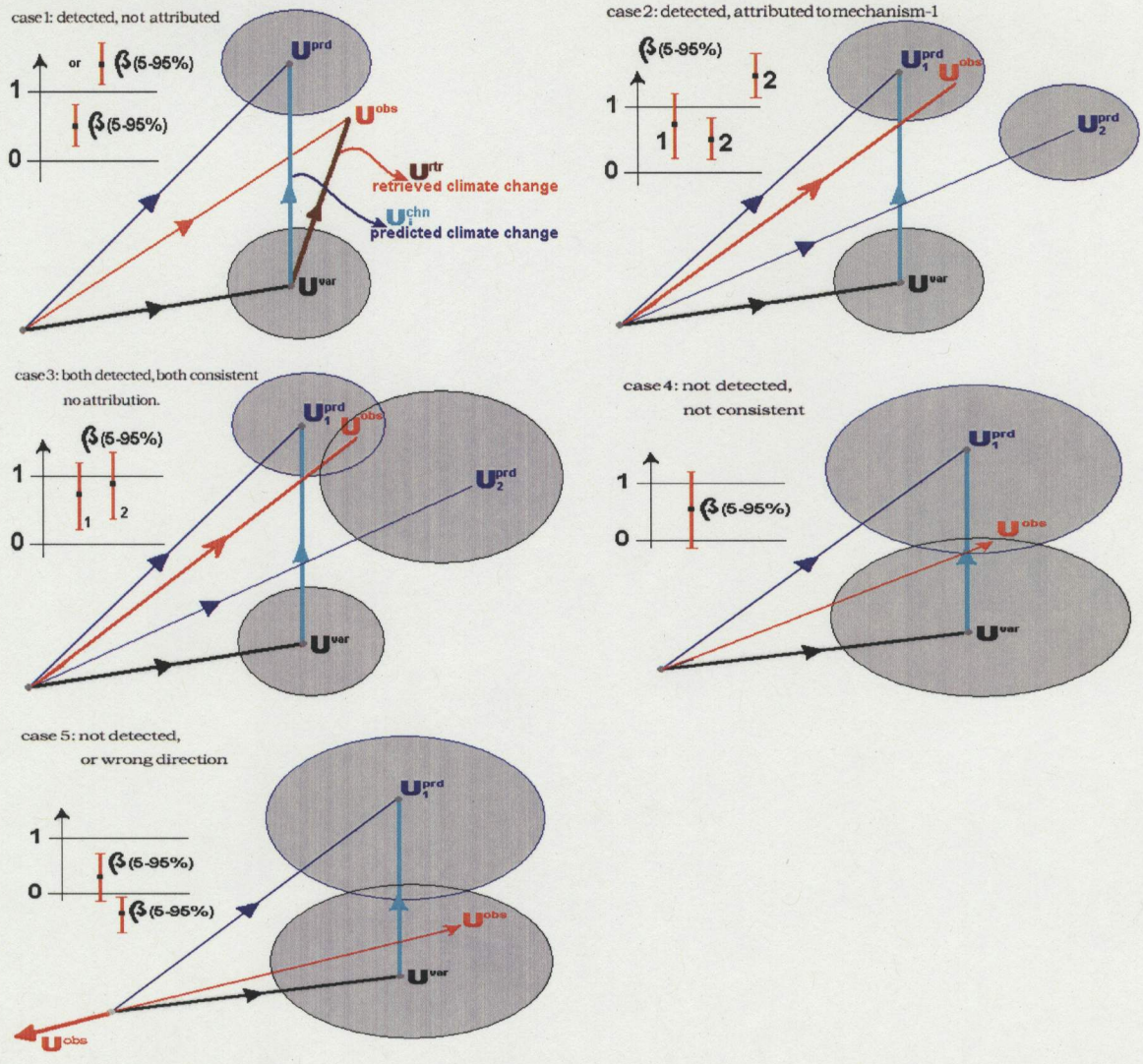

Figure 3.2: **Vectors and shadows have the same meaning as in Figure 3.1, the vertical bar on best guess of β shows its 5-95% confidence interval.**

3.2 Methodology of optimal fingerprinting used in climate change detection study

To understand the information in the subsequent Sections 3.3 and 3.4, the concepts and components related to the methodology, optimal fingerprinting, are introduced in this section.

"Fingerprinting" is the process of distinguishing internal climate variability from externally forced climate signal patterns (Barnett and Schlesinger 1987). In optimal fingerprinting, an optimal space-time-dependent linear filter function is applied to observed or simulated climate signals to maximize the signal-to-noise ratio (Hasselmann 1993). Figure 3.3 illustrates the rotation of the original signal to reach the maximized signal-to-noise ratio (Mitchell et al. 2001). There are other optimal approaches which have the same essential ideas as that of Hasselmann (1993, 1997) for the same purpose (Hegerl and North 1997). These approaches are the optimal weighting approach by Bell (1982, 1986) and the optimal filtering approach by North et al. (1995). In Hasselmann (1993), the fingerprint is given by the product of the assumed signal pattern and the inverse of the climate variability covariance matrix. If using Empirical Orthogonal Function (EOF) representations, the weighting factor is then replaced by the inverse of the square of the noise eigenvalues in order to scale the signal in the direction of low-noise EOFs (Santer et al. 1993). In Allen and Tett (1999) and Allen and Stott (2003), the optimal process is reached through introducing a pre-whitening coordinate transformation to the linear system. The detailed description of the optimal fingerprinting methodology can be found in Hasselmann (1993, 1997) and Allen and Stott (2003).

A multi-linear least squares solution of the above problem has been given by Allen and Tett (1999), Stott et al. (2001) (Ordinary Least Squares solution) and Mitchell et al. (2001), Allen and Stott (2003) (Total Least Squares solution). This solution explicitly quantifies the relationship between the model simulated signal and the observed signal. Assuming that the observations $\mathbf{y}$ can be expressed as a linear sum

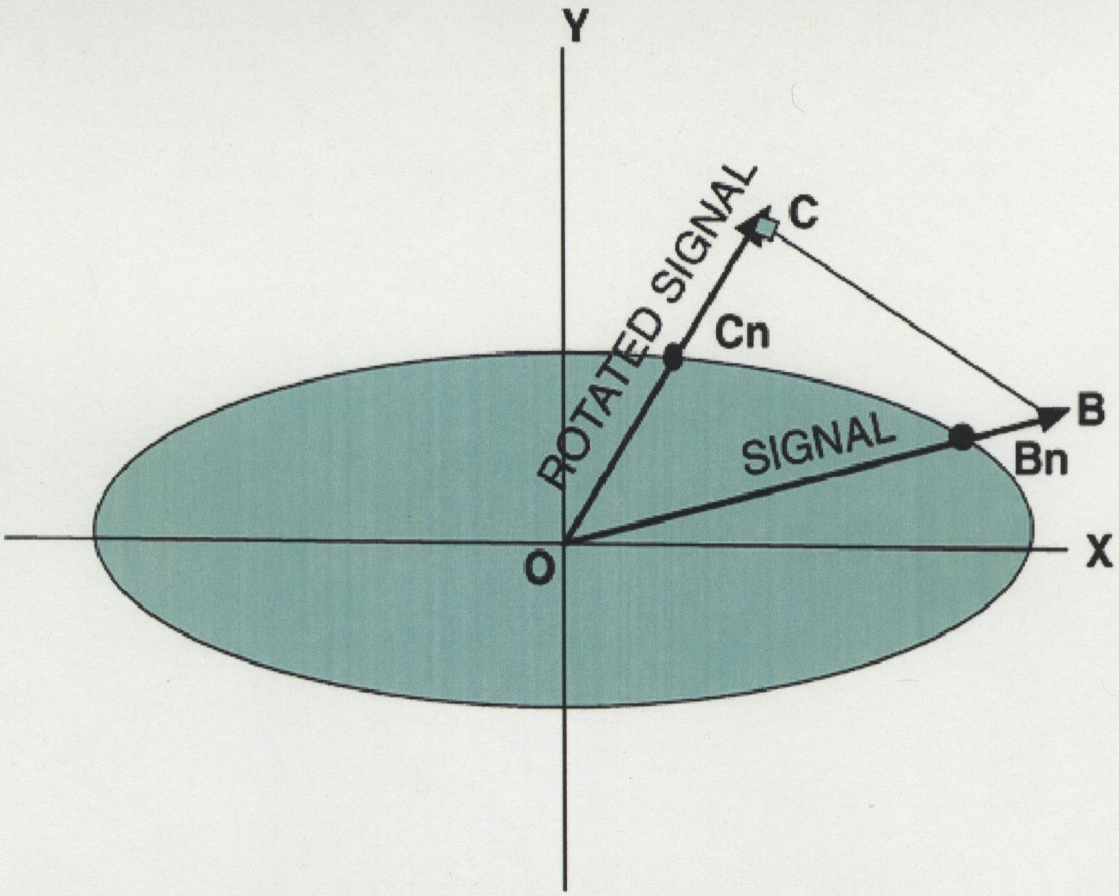

Figure 3.3: **An illustration of the rotation of the original signal to obtain the maximal signal-to-noise ratio. The shaded area is the 95% confidence region where the amplitude of the two spatial patterns of internal variability along OX and OY lie. There is a signal along OB whose signal-to-noise ratio is given by OB/OBn, OC is OB's projection along OC direction, the signal-to-noise ratio OC/OCn is larger than OB/OBn, since OB lies close to the direction of the main component of variability, while OC overlaps less with this main component. Therefore, the OC direction will be chosen to conduct the optimal detection. Reprinted from Box12.1 of Mitchell et al. (2001).**

of the scaled simulated responses to external forcings $\mathbf{x}$, and residual variability $\mathbf{u}$, then:

$$\mathbf{y} = \mathbf{x}\beta + \mathbf{u}. \tag{3.2}$$

In OLS, $\mathbf{x}$ is typically obtained from an ensemble of transient climate simulations of the 20th century involving greenhouse gases, aerosols, and other external forcing changes (based on estimates of historical forcing changes over the 20th century). In

TLS, $\mathbf{x}$ is the noise-reduced response pattern which is obtained from a hypothetical infinite ensemble, i.e. $\mathbf{x}$ should be represented as the difference between the finite model responses and an additional noise term. β is assumed to be a constant over the period of interest (Berliner et al. 2000). The best guess of β is calculated by minimizing the estimated least squares residual from the true signals, while the significance (for example, 90% confidence limits) of β are estimated based on the assumed distribution of the internal variability.

The conclusions about the signal detection and signal attribution can be drawn based on the amplitude of the regression coefficient β (Figure 3.2). The externally forced signal pattern is said to be detected in the observed data if the estimate of β is significantly greater than zero. Otherwise, the observed changes might be caused by other mechanisms like natural internal climate variabilities or forcings that are not included in the simulations. The attribution of a detected climate change signal to a particular forcing agent is obtained if the amplitude of β is consistent with unity, that is, the observed signal is consistent with the model-simulated response to the specified external forcing, after accounting for all plausible forcing agents. "The scaling factor β adjusts the signal amplitude so that the scaled signal best matches the observations" (Zwiers and Zhang 2003). The forced simulation underestimates the amplitude of the observed signal if $\beta > 1$ while it overestimates the observed signal if $\beta < 1$ (Mitchell et al. 2001).

3.3 Observed data and model outputs used in the climate change detection study

In this thesis, a five-decade sequence of decadal mean regionally-averaged surface air temperatures will be used as the detection variable (detector) to conduct an optimal detection study through an OLS method. This five-decade sequence covers the period from 1946 to 1996. The three temperature-related components necessary for a successful climate change detection study will be introduced in this section. These

three components are (1) the internal variability of temperature, (2) the observed temperature change signal, and (3) the simulated (predicted) temperature change signal.

As indicated in Section 3.1, it may not be appropriate to estimate internal variability from the observed temperature records. Therefore simulations from three climate models: PCM (Washington et al. 2000), HadCM2 (Johns et al. 1997), and CGCM2 (Flato and Boer 2001), are used as an alternative to estimate the internal variability. These climate models include control integrations of 1009 years with PCM, 1700 years with HadCM2, and 1000 years with CGCM2. The long control simulations of each model are used to estimate the covariance matrix of the internal climate variability. This matrix is used to derive the EOF basis for truncation of the signal patterns and signal-to-noise optimisation (Gillett et al. 2002). Since the decadal means of regionally averaged temperatures are used in this study, the data vector starts out with dimension 5, five EOFs are thus used without doing any dimension reduction. The model control runs are also used to estimate the uncertainty range of the regression coefficient β.

Each of these three models also has several transient integrations with either greenhouse gas (G) forcing, or combined GS (greenhouse gases and and sulfate aerosols) forcing, which are available for estimating optimal fingerprints of temperature changes for the second half of the 20th century. In this thesis, only the separate GSO (O: ozone) forcing runs of PCM are available, the separate GS runs are not available. However, the surface warming influence of ozone is too small to offset the cooling effect of sulphate aerosols. That is, a GS simulation of PCM will be nearly the same as the GSO run of PCM. Therefore, when analyzing the responses to GS forcing in PCM, actually the GSO forcing results are used and the O forcing is assumed to be so small that can be neglected.

For each model, the transient run outputs are averaged to reduce the noise generated by simulated signals based on the natural climate variability. Unfortunately this average still cannot avoid all sampling errors. The fields of each model are masked in the same manner as the observations so that places without adequate observations are

masked out of the model output. Mitchell et al. (2001) confirmed that the warming in the latter half of the 20th century is unlikely to be explained by the combination of internal and naturally forced climate variability. Therefore, similar to Gillett et al. (2002), this study regresses five optimised observed decadal-mean surface temperature anomalies (1946 – 1956, 1956 – 1966, 1966 – 1976, 1976 – 1986, 1986 – 1996) onto the G or GS simulated anomaly patterns of surface temperatures over the same period. A mean temperature anomaly over each region is taken and a total least squares fit is used to estimate β (Allen and Stott 2003). The best guess of β is calculated by minimizing the estimated least squares residual from the true signals, while the 90% confidence limits for β are estimated based on the assumed normal distribution of the internal variability, i.e., control integration of climate models, since both observed and simulated signal associated uncertainties arise from climate noise contamination (Hegerl et al. 1997).

3.4 Results

The regression coefficients of the GS forcing experiments for the seven biotic regions are shown in Figure 3.4. The regression coefficients are significantly different from zero, except for the tropical forest regions in the HadCM2 case, the tundra regions in the PCM case, and the ice region in all three models. This implies that the observed temperature changes are not likely to be explained by natural climate variability alone. The significant positive values of β over these regions suggest that an anthropogenic influence is detected in these cases. Both PCM and CGCM2 significantly overestimate the amplitude of the temperature anomaly response to the combined influence of increased greenhouse gases and sulphate aerosols in the water and tropical forest regions. An overestimation is also found in cultivated land regions by PCM. For the temperate forests and bare ground regions, the regression coefficients are significantly consistent with unity in all three models. This implies that the observed temperature changes in these two regions may be caused by changes in atmospheric greenhouse gas and sulphate aerosol concentrations.

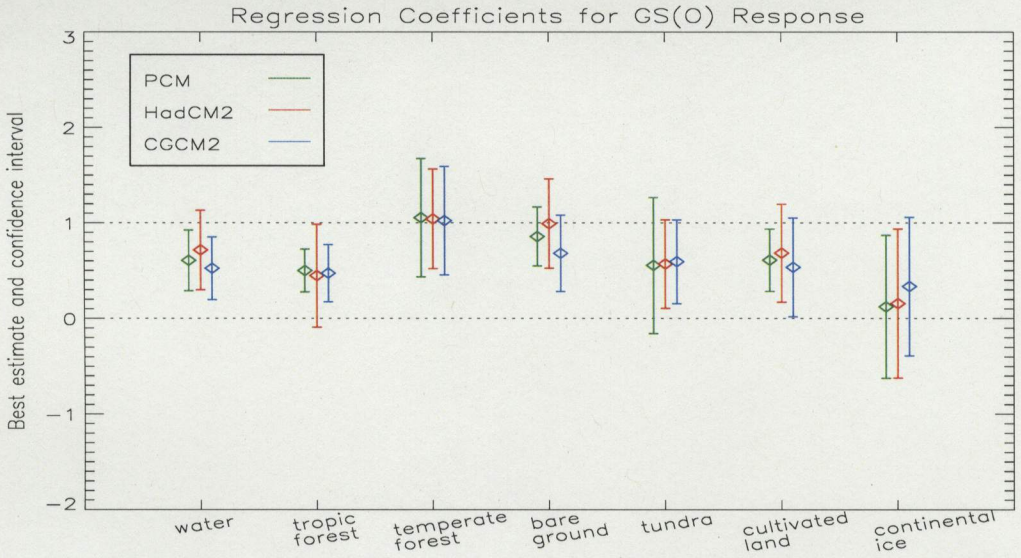

Figure 3.4: **Best estimate of the regression coefficients β and their 5-95% uncertainty ranges, of observed surface temperature changes against simulated changes in three climate models forced by external forcings. External forcings are combined GS in HadCM2 and CGCM2, and combined GSO in PCM.**

In Figure 3.4 we can also see that the uncertainty in the scaling factors varies between models. This follows since the simulated internal climate variability also varies between the models. The width of the uncertainty bars also tends to increase with a decrease in effective spatial scale of the land surface class (IDAG - International ad hoc Detection and Attribution Group 2005). This is further amplified in regions where there is a lack of observational data. Nevertheless, estimates of the regression coefficients using different models are similar to each other in all regions. This consistency provides enhanced confidence in the detection of an anthropogenic influence on regional warming.

We can further search for the detection of a greenhouse gas signal in the observed temperature record over the different vegetation classes (Figure 3.5). With the exception of the tropical forest in HadCM2, tundra in PCM, and continental ice in all three models, a greenhouse gas influence on surface temperatures is found to be detectable. G alone forced climate models generate an overestimation of surface temperatures. In this study, in regions where the G alone signal has been detected, the upper limits

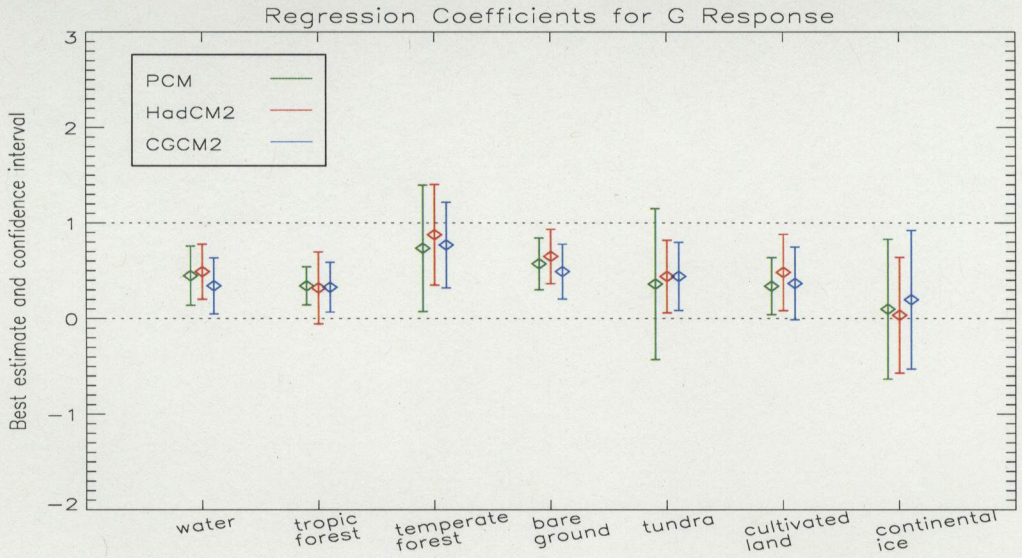

Figure 3.5: **Best estimate of the regression coefficients β and their 5-95% uncertainty ranges, of observed surface temperature changes against simulated changes in three climate models forced by external forcings. External forcings are greenhouse gas alone.**

of β are less than one. The three models typically overestimate the warming signal and provide results that are remarkably consistent with each other like before. Still for these regions, the amplitudes of the estimates of β from the combined GS forcing detection are generally closer to unity. This phenomenon can be explained by the compensation of the cooling effect of sulphate aerosols to the greenhouse gas warming effect on surface temperatures. External forcing that includes both G and S is closer to the real forcing in the atmosphere than G-forcing alone.

A two-way detection analysis using outputs from G simulations along with outputs from GS simulations relaxes the assumption that the relative magnitude of the G and S response is correctly simulated by the climate model (Gillett et al. 2002). In this case, Equation 3.2 has the form $\mathbf{y} = \beta_G \mathbf{x}_G + \beta_S \mathbf{x}_S + \mathbf{u}$ and an OLS regression is used here. According to Gillett et al. (2002), the estimated response to S forcing in each model is often computed as the difference between its GS simulation and G simulation, as a linear assumption generally is appropriate (personal communication with Nathan Gillett). Here both the integrations from the three individual models and a multi-model approach are used to separately estimate the amplitudes of the G and

Table 3.1: **Separately detected G and S signals in surface class based warming by three climate models and the multiple model**

Surface class number	Surface class type	HadCM2	CGCM2	PCM	Multi-model
1	Water	G	G	G	G
2	Tropic forest	–	G,S	G,S	G
3	Temperate forest	G,S	G	G,S	G
4	Bare ground	G	G	G,S	G
5	Tundra	G	G	–	G
6	Cultivated land	G	–	G,S	G,S
7	Continental ice	–	–	–	–

S regression coefficients, through a two-way regression approach. In the multi-model approach, two GS and two G forced simulations from all the three individual models are used to estimate the scaling factors. In addition, 800 years of control segments from all the three individual models (CGCM2, HadCM2 and PCM) are concatenated to derive the EOF basis and to estimate the uncertainties of the regression coefficients.

G or S are listed in Table 3.1 if either pattern has been detected. The signal from greenhouse gases G has been separately detected in at least two individual models over every vegetation type except continental ice. G has also been detected over all regions but the continental ice by the multi-model approach. For G, the multi-model results provide a consensus between the individual model results. S signal is separately detectable by PCM for all land regions except continental ice. Although S signal is not strong in other individual or multi-model cases, as we can expected, the detection of S over water region is failed since the influence of S is usually in land area within a short term.

To examine whether the observed temperature changes can instead be explained by natural climate influences such as changes in solar radiation or volcanic activities, we repeated the detection analysis using the solar and volcanic runs of PCM and checked whether the residual test that the control run of the model adequately can represent the variability of the observed temperature in the real world failed over each region. The results show that none of the regression coefficients, within its 90% con-

fidence range, are found to be positive in all seven regions and thus natural forcing is not detectable in the observed temperature change (Figure 3.6). The failure of residual tests tells us that natural forcings alone do not provide an adequate explanation of the observed temperature changes in all the seven biotic regions.

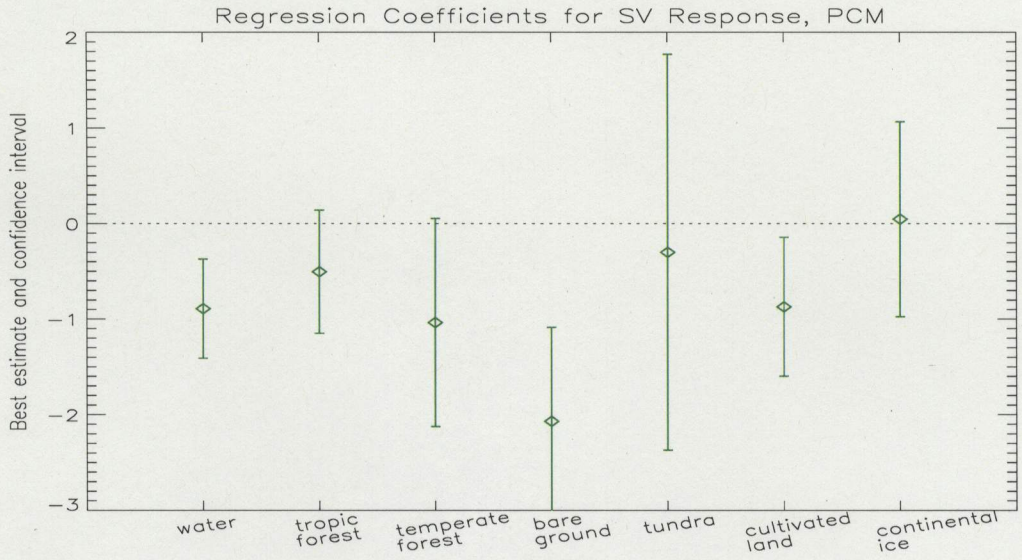

Figure 3.6: **Best estimate of the regression coefficients β and their 5-95% uncertainty ranges, of observed surface temperature changes against simulated changes in PCM forced by external forcings. External forcings are solar and volcanic influences.**

Chapter 4

Conclusions

The evolution of local biota as well as the influences of local climate are closely related to local surface temperature changes. Since surface temperatures at regions smaller than continental scales display both warming and cooling trends in the past century, and this divergence has been found over regularly divided regions of the globe (Giorgi 2002), the surface temperature trends at biotic regions are also expected to vary. The subsequent influences of these climatic changes on bio-systems may be very different from region to region. It is therefore necessary to examine how the instrumental surface temperature changes over major biome regions, as this examination has not been systematically conducted. It is also necessary to determine if there have been detectable signals of anthropogenic activities in these regions showing temperature changes. If there are, we may then be able to conclude that the substantial changes in ecosystems over the corresponding period may be due to anthropogenic influences. This study is also valuable for studies on climatic effects on future ecosystem evolution such as shifts of plant distribution and wild animal habitat.

The detection of warming or cooling trends and the extent to which the trends are controlled by the anthropogenic emission of greenhouse gases and sulphate aerosols was examined here. The analysis of instrumental records of surface temperatures revealed pronounced warming trends over the major biotic regions on Earth, starting from the beginning of the 20th century. Superimposed upon this overall global warming trend were some periods of regional cooling.

Using three different climate models we found a detectable combined anthropogenic greenhouse gas and sulphate aerosol signal over water, tropical forest, temperate forest, bare ground, tundra and cultivated land regions. The warming effect of greenhouse gases alone on surface temperatures is also detectable over different

regions by all climate models. Over every vegetation type except tundra and continental ice, at least two climate models have separately detected the influence of greenhouse gases. The G signals in six regions except continental ice have also been detected through a multi-model approach. S signal is separately detectable by PCM for all land regions except tundra and continental ice. The observed temperature changes in all the seven regions can not be explained by natural forcing alone.

Observed regional climate change signals are consistent with combined G and S forcing over temperate forest, bare ground, and tundra both in three separate climate models and in the multiple model. The same consistency has been found over cultivated land regions by both HadCM2 and CGCM2, while over global water, a consistency between climate change signal and GS forcing can only be found in HadCM2. We found that over temperate forest regions, the observed warming trend during the latter half century is also consistent with a greenhouse gas forcing mechanism alone by all three models through both the one-signal detection and two-signal detection. This consistency has also been revolved by the multi-model approach. Although regional scale climate features simulated by climate models are not as reliable as those at a global scale (Hasselmann 1993), the rather remarkable inter-model consistency of our detection results increases our overall confidence in the detectability of the anthropogenic signals at surface-type-based regional scales.

References

Ahrens, C. D. (1994). *Meteorology Today.* West Publishing Company, fifth edition.

Allen, M. R. and Stott, P. A. (2003). Estimating signal amplitudes in optimal fingerprinting, part 1: Theory. *Clim. Dyn.*, 21:477–491.

Allen, M. R. and Tett, S. F. B. (1999). Checking for model consistency in optimal fingerprinting. *Clim. Dyn.*, 15:419–434.

Barnett, T. and Schlesinger, M. (1987). Detecting changes in global climate induced by greenhouse gases. *J. Geophys. Res.*, 92:14772–14780.

Barnett, T. P., Hasselmann, K., Chellian, M., Delworth, T., Hegerl, G., Jones, P., Rasmusson, E., Roeckner, E., Ropelewski, C., Santer, B., and Tett, S. (1999). Detection and attribution of recent climate change: a status report. *Bull. Amer. Meteo. Soc.*, 80(12):2631–2659.

Barnett, T. P., Pierce, D. W., and Schnur, R. (2001). Detection of anthropogenic climate change in the world's oceans. *Science*, 292:270–274.

Bell, T. L. (1982). Optimal weighting of data to detect climatic change: Application to the carbon dioxide problem. *J. Geophys. Res.*, 87(11):161–170.

Bell, T. L. (1986). Theory of optimal weighting of data to detect climatic change. *J. Atmos. Sci.*, 43(16):1694–1710.

Berliner, L. M., Levine, R. A., and Shea, D. J. (2000). Bayesian climate change assessment. *J. Clim.*, 13:3805–3820.

Cubasch, U., Meehl, G. A., Boer, G. J., Stouffer, R. J., Dix, M., Noda, A., Senior, C. A., Raper, S., and Yap, K. S. (2001). Projections of future climate change. In Houghton, J., Ding, Y., Griggs, D., Noguer, M., van der Linden, P., Dai, X.,

Maskell, K., and Johnson, C., editors, *Climate Change 2001. The Scientific Basis Contribution of Working Group 1 to the Third Assessment Report of the Intergovernmental Panel on Climate Change*, pages 527–582. Cambridge University Press.

DeFries, R. S. and Townshend, J. R. G. (1994). Ndvi-derived land cover classification at global scales. *International Journal of Remote Sensing*, 15:3567–3586. Special Issue on Global Data Sets.

Doran, P., P., J. C., Lyons, W. B., Walsh, J. E., Lountain, A. G., McKnight, D. M., Moorhead, D. L., Virginia, R. A., Wall, D. H., Clow, G. D., Fritsen, C. H., McKay, C. P., and Parsons, A. N. (2002). Antarctic climate cooling and terrestrial ecosystem response. *Nature*, 415:517–520.

Flato, G. M. and Boer, G. J. (2001). Warming asymmetry in climate change simulations. *Geophys. Res. Lett.*, 28:195–198.

Folland, C. K., Karl, T. R., Christy, J. R., Clarke, R. A., Gruza, G. V., Jouzel, J., Mann, M. E., Oerlemans, J., Salinger, M. J., and Wang, S. W. (2001). Observed climate variability and change. In Houghton, J., Ding, Y., Griggs, D., Noguer, M., van der Linden, P., Dai, X., Maskell, K., and Johnson, C., editors, *Climate Change 2001. The Scientific Basis Contribution of Working Group 1 to the Third Assessment Report of the Intergovernmental Panel on Climate Change*, pages 99–181. Cambridge University Press.

Gillett, N. P., Weaver, A. J., and Flannigan, M. D. (2004a). Detecting the effect of climate change on canadian forest fires. *Geophys. Res. Lett.*, 31(20).

Gillett, N. P., Wehner, M. F., Tett, S. F. B., and Weaver, A. J. (2004b). Testing the linearity of the response to combined greenhouse gas and sulfate aerosol forcing. *Geophys. Res. Lett.*, 31.

Gillett, N. P., Zwiers, F. W., Weaver, A. J., Hegerl, G. C., Allen, M. R., and Stott, P. A. (2002). Detecting anthropogenic influence with a multi-model ensemble. *Geophys. Res. Lett.*, 29(20).

Gillett, N. P., Zwiers, F. W., Weaver, A. J., and Stott, P. A. (2003). Detection of human influence on sea-level pressure. *Nature*, 422:292–294.

Giorgi, F. (2002). Variability and trends of sub-continental scale surface climate in the twentieth century. I. observations. *Clim. Dyn.*, 18:675–691.

Giorgi, F., Hewitson, B., Christensen, J., Hulme, M., Storch, H. V., Whetton, P., Jones, R., Mearns, L., and Fu, C. (2001). Regional climate information – evaluation and projections. In et. al., J. H., editor, *Climate Change 2001. The Scientific Basis Contribution of Working Group 1 to the Third Assessment Report of the Intergovernmental Panel on Climate Change*, pages 585–638. Cambridge University Press.

Hasselmann, K. (1993). Optimal fingerprints for the detection of time-dependent climate-change. *J. Clim.*, 6:1957–1971.

Hasselmann, K. (1997). Multi-pattern fingerprint method for detection and attribution of climate change. *Clim. Dyn.*, 13:601–611.

Hasselmann, K. (1998). Conventional and bayesian approach to climate-change detection and attribution. *Q. J. R. Meteorol. Soc.*, 124:2541–2565.

Hegerl, G. C., Crowley, T. J., Baurm, S. K., Kim, K. Y., and Hyde, W. T. (2003). Detection of volcanic, solar and greenhouse gas signals in paleo-reconstructions of northern hemispheric temperature. *Geophys. Res. Lett.*, 30(5).

Hegerl, G. C., Hasselmann, K., Cubasch, U., Mitchell, J. F. B., Roeckner, E., Voss, R., and Waszkewitz, J. (1997). Multi-fingerprint detection and attribution analysis of greenhouse gas, greenhouse gas-plus-aerosol and solar forced climate change. *Clim. Dyn.*, 13:613–634.

Hegerl, G. C., Jones, P. H., and Barnett, T. P. (2000). Effect of observational sampling error on the detection of anthropogenic climate change. *J. Clim.*, 14:198–207.

Hegerl, G. C. and North, G. R. (1997). Comparison of statistically optimal approaches to detecting anthropogenic climate change. *J. Clim.*, 10:1125–1133.

Hegerl, G. C., Zwiers, F. W., Stott, P. A., and Kharin, V. V. (2004). Detectability of anthropogenic changes in temperature and precipitation extremes. *J. Clim.*, 17:3683–3700.

Hughen, K. A., Eglinton, T. L., Xu, L., and Makou, M. (2004). Abrupt tropical vegetation response to rapid climate changes. *Science*, 304:1955–1959.

IDAG - International ad hoc Detection and Attribution Group (2005). Detecting and attributing external influences on the climate system: A review of recent advances. *J. Clim.*, 18:1291–1314.

Johns, T., Carnell, R., Crossley, J., Gregory, J., Mitchell, J., Senior, C., Tett, S., and Wood, R. (1997). The second hadley centre coupled ocean-atmosphere gcm: model description, spin-up and validation. *Clim. Dyn.*, 13:103–134.

Jones, P. D., Osborn, T. J., Briffa, K. R., Folland, C. K., Horton, E. B., Alexander, L. V., Parker, D. E., and Rayner, N. A. (2001). Adjusting for sampling density in grid box land and ocean surface temperature time series. *J. Geophys. Res.*, 106:3371–3380.

Karoly, D. and Wu, Q. (2005). Detection of regional temperature changes in surface temperature. *J. Clim.*, in press.

Karoly, D. J., Braganza, K., Stott, P. A., Arblaster, J. M., Meehl, G. A., Broccoli, A. J., and Dixon, K. W. (2003). Detection of a human influence on north american climate. *Science*, 302:1200–1203.

Levitus, S., Antonov, J. I., Wang, J., Delworth, T. L., Dixon, K. W., and Broccoli, A. J. (2001). Anthropogenic warming of earth's climate system. *Science*, 292:267–270.

Mann, M. E., Bradley, R., and Hughes, M. (1999). Northern hemisphere temperature during the past millenium: inferences, uncertainties, and limitations. *Geophys. Res. Lett.*, 26:759–762.

Mann, M. E. and Jones, P. D. (2003). Global surface temperatures over the past two millennia. *Geophys. Res. Lett.*, 30(1820).

McAvaney, B., Covey, C., Joussaume, S., Kattsov, V., Kitoh, A., Ogana, W., Pitman, A., Weaver, A., Wood, R., and Zhao, Z.-C. (2001). Model evaluation. In Houghton, J., Ding, Y., Griggs, D., Noguer, M., van der Linden, P., Dai, X., Maskell, K., and Johnson, C., editors, *Climate Change 2001. The Scientific Basis Contribution of Working Group 1 to the Third Assessment Report of the Intergovernmental Panel on Climate Change*, pages 471–523. Cambridge University Press.

Meissner, K., Weaver, A., Matthews, H., and Cox, P. (2003). The role of land-surface dynamics in glacial inception: A study with the uvic earth system model. *Clim. Dyn.*, 21:515–537.

Melillo, J. M. (1999). Warm, warm on the range. *Science*, 283:183–184.

Mitchell, J. F. B., Karoly, D. J., Hegerl, G. C., Zwiers, F. W., Allen, M. R., and Marengo, J. (2001). Detection of climate change and attribution of causes. In Houghton, J., Ding, Y., Griggs, D., Noguer, M., van der Linden, P., Dai, X., Maskell, K., and Johnson, C., editors, *Climate Change 2001: The Scientific Basis, Contribution of Working Group 1 to the Third Assessment Report of the Intergovernmental Panel on Climate Change*, pages 695–738. Cambridge University Press.

Moore, B., Gates, W. L., Mata, L. J., and Underdal, A. (2001). Advancing our understanding. In Houghton, J., Ding, Y., Griggs, D., Noguer, M., van der Linden, P., Dai, X., Maskell, K., and Johnson, C., editors, *Climate Change 2001: The Scientific Basis, Contribution of Working Group 1 to the Third Assessment Report of the Intergovernmental Panel on Climate Change*, pages 771–785. Cambridge University Press.

North, G. R., Kim, K.-Y., Shen, S. S. P., and Hardin, J. W. (1995). Detection of forced climate signals. part I: Filter theory. *J. Clim.*, 8:401–407.

North, G. R. and Stevens, M. J. (1998). Detecting climate signals in the surface temperature record. *J. Clim.*, 11:563–577.

O'Reilly, C. M., Alin, S. R., Plisnier, P., Cohen, A. S., and McKee, B. A. (2003). Climate change decreases aquatic ecosystem productivity of Lake Tanganyika. *Nature*, 424:766–768.

Parmesan, C. and Yohe, G. (2003). A globally coherent fingerprint of climate change impacts across natural systems. *Nature*, 421:37–42.

Peixoto, J. P. and Oort, A. H. (1992). *Physics of Climate.* American Institute of Physics Press.

Petit, J. R., Jouzel, J., Raynaud, D., Barnola, J., Basile, I., Bender, M., Chappellaz, J., Davis, M., Delaygue, G., Delmotte, M., Kotlyakov, V., Legrand, M., Lipenkov, V., Lorius, C., Pepin, L., Ritz, C., Saltzman, E., and Stievenard, M. (1999). Climate and atmospheric history of the past 420,000 years from the Vostok ice core, Antarctica. *Nature*, 399:429–436.

Philander, S. G. (1998). *Is The Temperature Rising?* Princeton University Press.

Prentice, I. C., Farquhar, G. D., Fasham, M. J. R., Goulden, M. L., Heimann, M., Jaramillo, V. J., Kheshgi, H. S., Quere, C. L., Scholes, R. J., and Wallace, D. W. R. (2001). The carbon cycle and atmospheric carbon dioxide. In Houghton, J., Ding, Y., Griggs, D., Noguer, M., van der Linden, P., Dai, X., Maskell, K., and Johnson, C., editors, *Climate Change 2001: The Scientific Basis, Contribution of Working Group 1 to the Third Assessment Report of the Intergovernmental Panel on Climate Change*, pages 185–237. Cambridge University Press.

Ramaswamy, V., Boucher, O., Haigh, J., Hauglustaine, D., Haywood, J., Myhre, G., Nakajima, T., Shi, G. Y., and Solomon, S. (2001). Radiative forcing of climate

change. the scientific basis. In Houghton, J., Ding, Y., Griggs, D., Noguer, M., van der Linden, P., Dai, X., Maskell, K., and Johnson, C., editors, *Contribution of Working Group 1 to the Third Assessment Report of the Intergovernmental Panel on Climate Change*, pages 351–406. Cambridge University Press.

Root, T. L., Price, J. T., Hall, K. R., Schneider, S. H., Rosenzweig, C., and Pounds, J. A. (2003). Fingerprints of global warming on wild animals and plants. *Nature*, 421:57–60.

Santer, B. D., Taylor, K. E., Wigley, T. M. L., Penner, J. E., Jones, P. D., and Cubasch, U. (1995). Towards the detection and attribution of an anthropogenic effect on climate. *Clim. Dyn.*, 12:77–100.

Santer, B. D., Wigley, T. M. L., and Jones, P. D. (1993). Correlation method in fingerprinting detection studies. *Clim. Dyn.*, 8:265–276.

Stott, P. A. (2003). Attribution of regional-scale temperature changes to anthropogenic and natural causes. *Geophys. Res. Lett.*, 30(14).

Stott, P. A. and Tett, S. F. B. (1998). Scale-dependent detection of climate change. *J. Clim.*, 11:3282–3294.

Stott, P. A., Tett, S. F. B., Jones, G. S., Allen, M. R., Ingram, W. J., and Mitchell, J. F. B. (2001). Attribution of twentieth century temperature change to natural and anthropogenic causes. *Clim. Dyn.*, 17:1–21.

Stott, P. A., Tett, S. F. B., Jones, G. S., Allen, M. R., Mitchell, J. F. B., and Jenkins, G. J. (2000). External control of 20th century temperature by natural and anthropogenic forcings. *Science*, 290:2133–2137.

Tett, S. F. B., Jones, G. S., Stott, P. A., Hill, D. C., Mitchell, J. F. B., Allen, M. R., Ingram, W. J., Jones, T. C., Johnson, C. E., Jones, A., Roberts, D. L., Sexton, D. M. H., and Woodage, M. J. (2000). Estimation of natural and anthropogenic contributions to 20th century. *Hadley Centre Tech Note 19, Hadley Center for Climate Prediction and Response*, RG12 2SY, UK:pp52.

Tett, S. F. B., Stott, P. A., Allen, M. R., Ingram, W. J., and Mitchell, J. F. B. (1999). Causes of twentieth-century temperature change near the earth's surface. *Nature*, 10:569–572.

Thomas, C. D., Cameron, A., Green, R. E., Bakkenes, M., Beaumont, L. J., Collingham, Y. C., Erasmus, B. F. N., de Siqueira, M. F., Graninger, A., Hannah, L., Hughes, L., Huntley, B., van Jaarsveld, A. S., an dL. Miles, G. F. M., Grtega-Huerta, M. A., Peterson, A. T., Phillips, O. L., and Williams, S. E. (2004). Extinction risk from climate change. *Nature*, 427:145–148.

von Storch, H. and Zwiers, F. W. (1999). *Statistical Analysis in Climate Research.* Cambridge University Press.

Washington, W. M., Weatherly, J. W., Meehl, G. A., Semtner, A. J., Bettge, T. W., Craig, A. P., Strand, W. G., Arblaster, J., Wayland, V. B., James, R., and Zhang, Y. (2000). Parallel climate model PCM control and transient simulations. *Clim. Dyn.*, 16(10-11):755–774.

Weaver, A. J. and Zwiers, F. W. (2000). Uncertainty in climate change. *Nature*, 407:571–572.

Wuebbles, D. J. and Hayhoe, K. (2001). Atmospheric methane and global change. *Earth-Sci. Rev.*, 57:177–210.

Zhang, X., Zwiers, F. W., and Stott, P. (2005). Multi-model multi-signal climate change detection at regional scale. *J. Clim*, submitted.

Zwiers, F. W. (2002). The 20-year forecast. *Nature*, 416:690–691.

Zwiers, F. W. and Zhang, X. (2003). Toward regional-scale climate change detection. *J. Clim.*, 16(5):793–797.

Appendix A

An idealized greenhouse effect model

This model is taken from Philander (1998) while physical laws and constants in the solution are taken from Peixoto and Oort (1992). In this model, Earth is assumed to be a blackbody, the isothermal atmosphere is assumed to be entirely transparent to incident solar radiation and "black" to infra-red radiation, as the greenhouse gases in the atmosphere have the ability to trap long-wave energy emited from both the Earth's surface and from those components inside the atmosphere such as clouds.

Stefan-Boltzmann Law: $Q = \sigma T^4$, where $\sigma = 5.67 \times 10^{-8} W m^{-2} K^{-4}$.

Q_{in}: incident solar flux (solar constant), assumed to be $1370 W/m^2$;

Q^*: the average solar flux reached at the top of the atmosphere;

R: radius of Earth;

T_E: the Earth's surface temperature;

Q_E: the energy received at Earth's surface;

α: planetary albedo of Earth, assumed to be 0.3;

The Earth intercepts solar radiation like a disk with a radius R, thus total solar radiation received by Earth is $E = \pi R^2 Q_{in}$ E is also equal to the total solar energy received by the spherical Earth, i.e. $E = 4\pi R^2 Q^*$, then $Q^* = 0.25 Q_{in}$. Therefore, Q, the average solar flux being absorbed by the Earth-atmosphere system is $Q = Q^*(1 - \alpha) = Q^*(1 - 0.3) = 1370 \times 0.25 \times 0.7 = 239.75 W/m^2$.

A.1 No atmosphere – no greenhouse gases

The temperature of the Earth's surface is determined by the amount of energy it receives. As Earth is assumed to be a blackbody, the energy it receives is only solar radiation which is $Q = 239.75 W/m^2$. Applying Stefan-Boltzmann Law, $Q = \sigma T^4$,

the Earth's surface temperature is $T_E = \sqrt[4]{239.75/\sigma} = 255.0022K = -17.9978$°C.

A.2 One layer atmosphere – with normal greenhouse gas concentration

Considering the greenhouse gases, the energy arriving at the Earth's surface includes both incoming sunlight and the emission of infra-red light. Over a long term equilibrium, the Earth-atmosphere system must radiate as much energy out as it receives from the sun, i.e. $Q = Q_{out}$ (left panel of Figure A.1). Since the atmosphere is isothermal, the temperature at the top of the atmosphere is same as that at the bottom, thus, $Q_{out} = Q^*_{out}$.

The energy received at the Earth's surface is then $Q_E = Q + Q^*_{out} = 2Q$. According to Stefan-Boltzmann Law, (Energy equilibrium at Earth's surface is $Q' = Q + Q^*_{out}$)

$$T_E = \sqrt[4]{Q_E/\sigma} = \sqrt[4]{2 \times Q/\sigma} = \sqrt[4]{2 \times 239.75/(5.67 \times 10^{-8})} = 303.25K = 30.25$$

°C

Although 30.25°C is much larger than the observed surface air temperature 15°C, this result has clearly illustrated the influence of the greenhouse gases.

A.3 Two layer atmosphere – with doubled doubled greenhouse gases

Here the doubling of the greenhouse gas concentration is simply assumed to add another layer of isothermal atmosphere (right panel of Figure A.1). Applying the Stefan-Boltzmann law and consider the equilibrium of radiation energy at the Earth's surface, at the top of the atmosphere, and in the two layers of atmosphere. When greenhouse gas concentration is doubled, the earth surface temperature will almost be doubled as well, as solved in the following paragraph. Note that a tribled greenhouse

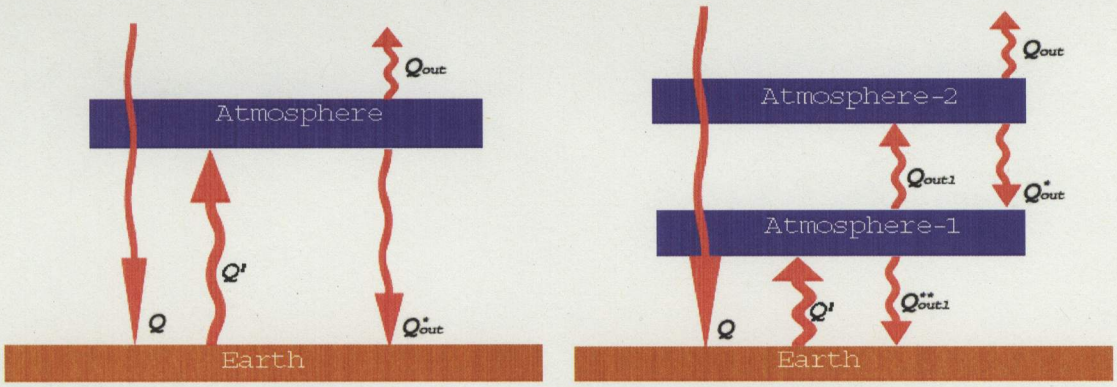

Figure A.1: **An idealized model of the greenhouse effect in Earth's atmosphere. Atmosphere is assumed to be isothermal and entirely transparent to sunlight, it is also assumed to be entirely opaque to the infra-red heat. The left panel is for the normal greenhouse gas concentration in Earth's atmosphere. The right panel illustrates the atmosphere with a doubled greenhouse gas concentration.**

gas will not induce the surface temperature to be tribled by this model.

Similar to the analysis in section A.2, $Q = Q_{out}$, then $Q_{out} = Q^*_{out}$. Since the layer "Atmosphere-2" receives Q_{out1} and radiates out $2Q_{out}$, $Q^{**}_{out1} = Q_{out1}$ and $Q_{out1} = Q_{out} + Q^*_{out} = 2Q_{out}$, the energy received at the Earth's surface is then $Q_E = Q + Q^*_{out} + Q^*_{out} = 3Q$. According to Stefan-Boltzmann Law,

$$T_E = \sqrt[4]{Q_E/\sigma} = \sqrt[4]{3 \times Q/\sigma} = \sqrt[4]{3 \times 239.75/(5.67 \times 10^{-8})} = 335.6K = 62.6$$

°C

After the abundance of the greenhouse gases is doubled, the Earth's surface temperature will be up to 62.6°C, about twice the surface temperature under the normal greenhouse gas condition. (Note: generally an additional 3 – 4°C are expected for CO_2 doubling in the real atmosphere on Earth).

A.4 Discussion of shortcomings

While the actual magnitude of the numbers in Section A.2 and A.3 are not meaningful, the simple model is illustrative of the processes involved in the greenhouse effect.

Compared to the real Earth-atmosphere system, there are several shortcomings in this model. For example, the assumption that the atmosphere is completely transparent to the incoming sunlight and completely "black" to the infra-red radiation causes too much radiation to be received on Earth. This is one reason why the computed surface temperature is higher than the observed average temperature of 15°C.

The second major shortcoming is that the atmosphere is completely transparent to incoming solar radiation. This assumption has ignored the part reflected and scattered by clouds and O_3 in the atmosphere. This part doesn't reach the Earth's surface in reality. Therefore, this is another reason that causes a higher estimated temperature.

The third shortcoming is that the atmosphere is not isothermal, i.e. the temperatures at the bottom and top of the atmosphere are in fact different and outgoing radiations are also different. In addition, the effects of a doubled CO_2 climate can not be equivalent to adding another layer of atmosphere.

Although this idealized model is far from accurate for a real Earth-atmosphere system, it illustrates the greenhouse gas effect, and the influence of increased greenhouse gas concentrations in the atmosphere.

Appendix B

Derivation of optimal fingerprinting

In this section, the solution to the standard detection model (3.2) is given, i.e. estimating β by Total Least Squares (Mitchell et al. 2001, Allen and Stott 2003) or Ordinary Least Squares (Allen and Tett 1999, Stott et al. 2001).

The general representation of the regression model is:

$$\mathbf{y} = \mathbf{x}\beta + \mathbf{u}. \tag{B.1}$$

where, $\mathbf{y}$ is a column vector with rank l and represents the observed climate change signal. $\mathbf{x}$ is a $l \times n$ matrix, with n columns of externally forced signal patterns. In OLS, $\mathbf{x}$ is the n finite model-simulated response patterns. In TLS, $\mathbf{x}$ is the noise-free response pattern which is obtained from a hypothetical infinite ensemble, i.e. $\mathbf{x}$ should be represented as the difference between the finite model responses and an additional noise term.

β is a column vector with n scaling factors for n response patterns in $\mathbf{x}$. $\mathbf{u}$ is a column vector with rank l, its covariance matrix $\mathbf{C_N}$ (Equation B.2) can be estimated from long control runs of climate models (Section 3.3). $\mathbf{u}$ can be assumed to have a multivariate normal distribution (Section 3.1). $\mathbf{C_N}$ is not equal to $\sigma^2 I$. The estimated errors in β will be strongly biased when applying the unweighted least squares regression (Allen and Stott 2003). To avoid this problem and find the lowest variance estimator of β, a "pre-whitening" operator – coordinate transformation P

with rank k is introduced (Equation B.3).

$$\mathbf{C_N} \equiv \epsilon(\mathbf{u}\mathbf{u}^\mathbf{T}) \tag{B.2}$$

$$\epsilon(\mathbf{P}\mathbf{u}\mathbf{u}^\mathbf{T}\mathbf{P}^\mathbf{T}) = \mathbf{I} \tag{B.3}$$

$$\mathbf{P}^\mathbf{T}\mathbf{P} = \mathbf{C}_\mathbf{N}^{-1} \tag{B.4}$$

If C_N^{-1} exists, then Equation B.3 is satisfied.

Note ϵ is the expetation operator. In climate models, the small-scale noise variance usually is poorly simulated, therefore, k is then usually smaller than l.

Pu is independent, identically distributed (i.i.d), it is indistinguishable from white noise.

Assume $\epsilon(\mathbf{u}) = \mathbf{0}$, there is,

$$\epsilon(\mathbf{y}) = \epsilon(\mathbf{x}\beta) + \epsilon(\mathbf{u}) = \mathbf{x}\beta \tag{B.5}$$

The sum of the squared residuals are then minimized, in optimal treatment and, the transformed **u** substituted for the original **u**. Here it is to minimize $\|Pu\|^2$. Substitute the Equation B.1 into this expression, there is, $\|Pu\|^2 = \|P(y - x\beta)\|^2$. Set the derivate of the expression with respect to β equal to zero and solve for β, we have:

$$\widetilde{\beta} = (\mathbf{X}^\mathbf{T}\mathbf{P}^\mathbf{T}\mathbf{P}\mathbf{X})^{-1}\mathbf{X}^\mathbf{T}\mathbf{P}^\mathbf{T}\mathbf{P}\mathbf{y} = (\mathbf{X}^\mathbf{T}\mathbf{C}_\mathbf{N}^{-1}\mathbf{X})^{-1}\mathbf{X}^\mathbf{T}\mathbf{C}_\mathbf{N}^{-1}\mathbf{y} \equiv \mathbf{F}^\mathbf{T}\mathbf{y} \tag{B.6}$$

We have assumed that the model simulated signal **x** is true, i.e. all potential uncertainties in **x** have been included in the uncertainties in **u**. Since **u** is multivariate normally distributed, $\widetilde{\beta}$ also has a multivariate normal distribution with the mean β and the inflated covariance $(1+1/M)\mathbf{V}(\widetilde{\beta})$, where, M is the number of transient runs ensembled to reduce the variance of the forced response pattern.

$$\beta = \epsilon(\widetilde{\beta}) \tag{B.7}$$

$$\mathbf{V}(\widetilde{\beta}) = \epsilon(\widetilde{\beta} - \beta)(\widetilde{\beta} - \beta)^\mathbf{T} = (\mathbf{X}^\mathbf{T}\mathbf{P}^\mathbf{T}\mathbf{P}\mathbf{X})^{-1} = (\mathbf{X}^\mathbf{T}\mathbf{C}_\mathbf{N}^{-1}\mathbf{X})^{-1} \tag{B.8}$$

Equation B.8 then implies that a $(1-\alpha) \times 100\%$ confidence region for β is given by

$$(\widetilde{\beta} - \beta)^{\mathbf{T}} \mathbf{X}^{\mathbf{T}} \mathbf{C}_{\mathbf{N}}^{-\mathbf{1}} \mathbf{X} (\widetilde{\beta} - \beta) \leq \chi^{\mathbf{2}}_{\mathbf{1}-\alpha} \tag{B.9}$$

Where $\chi^2_{1-\alpha}$ is the $(1-\alpha)$ critical value of the chi-squared distribution with n degrees of freedom. For one-signal detection, if the lower limit confidence interval is positive, then the signal is said to be detected at the $\alpha/2 \times 100\%$ significance level. For two-signal detection, the observed change signal is said to be consistent with the two external forcing mechanism if the confidence ellipsoid contains the unit vector.